

## **Response to Reviewer RC1 – Prof. Ed Bueler**

### **Egusphere-2024-1052 Article**

#### **Author Responses in Red**

**I thank Prof. Bueler for a detailed and helpful review!**

Summary: This paper rewrites the standard glaciological (Glen law) Stokes model in a form which resembles a shallow approximation, the Blatter-Pattyn (BP) model. This expresses the saddle-point structure of the Stokes problem in a form close to the unconstrained-optimization form of the BP model. The stability and finite element (FE) analysis of the new form is addressed, and new mixed FE pairs for vertically-extruded meshes are proposed. Small-scale experiments are presented, and then prospective applications at larger scale are discussed. The resulting essentially-theoretical paper is both frustrating and promising. The manuscript's current form is notably inefficient, with 1500 lines of text. The presentation is likely to be hard to read for those who have not already done battle with BP equations and related technical matters. Despite doing numerical experiments, the author provides no open-source code basis for further development by readers, a clear demerit in 2024. The manuscript avoids the function-space understanding of the Stokes and BP problems---this is the viewpoint from which these problems are known to be well-posed and by which they are solved by mainstream finite element libraries---but then it labors to build a fragmented substitute for this viewpoint. Despite these flaws, the paper illuminates important matters. It shows how the (transformed) Stokes equations are close to an "extended Blatter-Pattyn" (EBP) form, and thereby how the solvability conditions of the Stokes model work in practice over vertically-extruded meshes. The EBP model has similar numerical and stability issues as the Stokes problem, which is actually clarifying because the numerical and FE character of the standard BP and Stokes models otherwise appear very different. The inf-sup stability of the mixed Stokes problem is recognized here, when the mesh is extruded and when one simultaneously wants the EBP model to be solvable on the same mesh, as the requirement of unique solvability of the continuity (incompressibility) equation for the vertical velocity from the horizontal velocity. A necessary condition for this to work is that the number of vertical velocity and pressure unknowns must be exactly the same, or rather that a particular matrix in the blockwise form of the discrete equations must be invertible.

Recommendation: A manuscript which made the same points in half the length, and which provided open source code in a widely-used language, facilitating further

August 28, 2024

development, would be an excellent paper. Of course it is not realistic to expect re-coding at that level. However, significant revisions should be attempted. A much-shortened abstract is offered below, along with several other suggestions for trimming.

An effort has been made to tighten and shorten the manuscript while preserving the content. The line count has been reduced to 1340 while preserving most of the content. Unfortunately, it is not possible to provide open source code in a widely used language because of the piecemeal way that the work was carried out using the Mathematica program, as pointed out in the paper.

#### Specific Comments on Manuscript

lines 9-35: This long abstract could be halved without losing meaning, by removing the sales pitches and by other simple edits. However, changes are also needed to clearly identify the models (systems) under consideration. The following is a guess/suggestion for an abstract which meets these objectives. It has 191 words vs 371 in the original: ""We introduce a novel transformation of the Stokes equations into a form that resembles the shallow Blatter-Pattyn (BP) equations. The two forms only differ by a few additional terms, and the variational formulations differ only by a single term in each horizontal direction, but the BP form also lacks the vertical velocity in the second invariant of the strain rate tensor. The transformed Stokes model has the same type of gravity forcing as the BP model, determined by the ice surface slope. An apparently intermediate "extended Blatter-Pattyn" (EBP) form is identified, which is actually the same as the standard BP model although it retains a pressure variable. The role played by the vertical velocity in the transformed Stokes and EBP forms, reflected in the block-wise structure of their discrete equations, motivates the construction of new finite element velocity/pressure pairs for vertically-extruded meshes. With these new pairs, examples of which are demonstrated in 2D and 3D, the discrete continuity equation can be uniquely and stably inverted for the vertical velocity. We describe how to incorporate the new forms into codes that adaptively switch between Stokes and BP models, where the latter would lose accuracy.""

I have rewritten the abstract using many of these suggestions. Thank you.

line 41: "full" is unnecessary.

Removed

line 52-72: The style of glaciology, used at unnecessary length in these lines, says some models are shallow and some are higher order. It is more accurate to say all are shallow, and to not claim some are "higher-order" because the order depends on which scaling argument is use.

I have used the term "shallow" only as part of the accepted names of some simple approximations. The term "higher-order" is commonly applied to the Blatter-Pattyn and other more accurate approximations.

line 99: "THE LOWER BOUNDARY OF an ice sheet ...". (A 3D ice sheet can't be divided the way the text says.) (1)

Don't quite understand what the problem is. This is an idealized situation of course. I will be glad to make whatever change is required.

lines 103-105: This "vertical line of sight" phrase appears here and later. Surely one can just say: "We assume the glacier's geometry is described by an upper surface function  $z_s(x,y)$  and a lower surface function  $z_b(x,y)$ ."

This was intended to mean that there should not be various indentations so that various multiple upper and lower surfaces would exist along a vertical line. Although unlikely, these could be handled but would complicate things considerably. I have changed this to say that there should be just one upper and one lower surface.

lines 105-106: There is nothing about the rest of the paper, in my reading, that excludes the techniques being used for floating ice. (Put  $f_i=0$  in equation (11)?) It is true that there must be sufficient drag--see the inequality in Schoof (2006)--\*somewhere at the base\* so that the velocity field is unique, but the techniques apply across grounding lines.

I have modified the sentence to say that ice shelves can be handled.

lines 112--126 Briefer notation is surely possible.

I have simplified by removing superscripts on unit normal vectors. Not sure what else can be done.

August 28, 2024

line 149: "positive-definite" --> "nonnegative"

Changed to "a positive quantity"

line 178-180: Whether or not the surface kinematical equations can be added "easily", the way this is said here is silly. The whole paper assumes fixed ice geometry.

Yes, fixed geometry is assumed. What this says is that flux inflows or outflows are allowed through a fixed geometry (which may be a crude representation of melting or refreezing at the bed).

lines 192-195: I don't know what this means. "There are some stress boundary conditions and it is easier for the author to think about them in the variational formulation."? No need for this?

This means that evaluating derivatives at boundaries is less accurate or more complicated because one-sided formulas have to be used due to the absence of information from across the boundary. I have changed the wording to make this clearer.

lines 197-200: No need for this.

I think this needs to be pointed out because most people use the weak formulation method and may not be familiar with the variational method.

lines 204-209: Is this option ever used later in the paper? (Line 233 suggests not.) If not, it can be removed and replaced with a simple declaration that the boundary conditions can be weakly imposed if desired.

I have indeed used it but most computations were done using direct substitution, as stated on Line 233. Of course, there is no difference in the results. However, it is a useful option and some people may prefer it. There are some consequences when Lagrange multipliers are used. For example, the "solvability condition" must be modified (see Line 626 in the originally submitted paper). For this reason, I prefer to leave this section as is.

lines 238-252: This is a valuable observation, namely form (17) which shows  $\sim P$  solves a trivialized problem. If this observation is original, then great. Otherwise cite it more clearly; did it appear in DPL 2010? (The nearby citations to DPL do not refer to this main idea as far as I can tell.)

August 28, 2024

It is original but only insofar as it refers to the transformed pressure ( $\tilde{P}$  not  $P$ ) in the Blatter-Pattyn approximation. It does not appear in DPL, 2010, since the new transformation was not invented yet.

Figure 2: This basic point is greatly appreciated: The deviation from hydrostatic is relatively small. However, in this and almost all figures, the fonts are too small! (Also these figures are bad on a monochrome printer, but I suppose that train has left ...) Changing all figures would be difficult. Should be OK for young eyes ....

line 282: I don't think (22) is actually used \*here\*.

Yes, it is used in the strain rate tensor (6) and in the second invariant (7). See (26) and (28).

around line 282: Warn the reader that "dummy variables" ("flag variables"?) are about to be used. As the text is written, they are finally explained on the next page.

Done

lines 286 and onward: I find "modified" really unpleasant here. For (25) the tensor  $\tilde{\tau}_{ij}$  is actually modified; it is not equal to the original. But in (26) the tensor is merely rewritten; neither "modified" nor the tilde have the same meaning as they do in the equation above. Similarly (27) and (28) are not "modified" but merely rewritten, as far as I can tell. I therefore would not say "modified" or add a tilde; just write out the new form. Equality means equality.

I must disagree here. Equations (26), (27), (28) are indeed modified because  $\partial w/\partial z$  is replaced by  $-(\partial u/\partial x + \partial v/\partial y)$  according to (22). They may have the same numerical value at convergence but they are discretized differently, so they are "modified". It is also important to distinguish quantities in the transformed Stokes equations from the standard or traditional Stokes to avoid confusion.

line 325: "implies the use of" --> "uses"

Done

lines 327-336: This is a rambling paragraph that can be shortened to something like "As noted earlier we require the upper and lower surfaces of the glacier to be functions of the

horizontal coordinates  $x,y$ . That is, as expected in glacier modeling, overhangs are not permitted."

Thank you, this is better. Text has been changed.

line 344-348: Repetitive. Say \*once\* (earlier, presumably) that one could impose boundary conditions weakly, and that you won't do that.

Shortened, but did mention can use Lagrange multipliers, if desired.

line 360: Help the reader by referencing/comparing (23).

I have referenced (23) and (25) following (37).

lines 361 and 404: Separate these into 2 displays. (Or better, just be more efficient. Use vector notation?)

I have done it this way in an effort to be more compact (long paper!) I think it's quite clear that I have combined equations and boundary condition. Vector notation would not be good because the rest of the paper uses Cartesian tensors.

lines 437-439: This use of the continuity equation is completely mainstream in glaciology. It applies in all shallow theories including BP. (And the current manuscript illuminates it!) Please say this some other way.

This has been reworded.

lines 459-460: Again, deriving FE discretizations from variational principles is the normal way to do business. Why "except"?

My understanding is that the normal way to do FE business is by means of the weak formulation.

line 475: There is no reason to use capital "U" here, and it is a source of confusion because capital U is used shortly in subscripts with a different meaning.

I have changed U to V.

line 495: "u, w, AND  $M_{\{UP\}}$ ,  $M_{\{WP\}}$ "

Section 4.3: This section needs editing most. The main point of the entire paper is made in subsection 4.3.3, I believe. Roughly-speaking the main point is that, for the

transformed Stokes or EBP equations, the block  $M_{\{WP\}}$  must be invertible, thus square, when an extruded mesh with z-aligned cells is used. This point is buried after laborious and repetitive text. The main point of the paper *does* require a block-wise presentation of the Newton step equations, so the text will necessarily be somewhat technical, but it doesn't have to bury the main idea. There would seem to be no reason not to start a section with (47) and (48); the notation here is obvious. In any case, this reader had to get 600 lines into the document before getting to the key lines (roughly starting at line 596), and only then have an "oh ... that is what he is trying to say ..." moment.

lines 596-600: The main point of the paper, right? Which this reader appreciates! The blockwise form of the EBP model is therefore the central object of the paper, and could be put much earlier and more prominently.

**Section 4.3 has been completely rewritten. I believe it may now address these comments.**

lines 616-618: I would not permit my undergrad linear algebra students to say what is said here. The necessary condition is that  $M_{\{WP\}}$  must be non-singular\*, from which it *follows logically* that it must be square. The text literally says that non-singularity is "in addition" to squareness, thereby asserting that square matrices are invertible! (Line 1521 is worse.) Equation (56) could instead say " $M_{\{WP\}}$  is non-singular"; one is allowed to put text in displayed LaTeX equations.

**I have been careless here. In Section 4.3.2 it now says: “matrix  $M_{WP}^T$  must be invertible and so it must be square and full rank. Since in general  $M_{WP}^T$  is an  $n_p \times n_w$  matrix, for solvability this requires that  $n_p = n_w$ ”.**

Section 5: I think the paper would be improved by removing this section. I understand that the transformed Stokes model is the same as the Stokes model, and the EBP model is the same as the BP model. So recapitulating the ISMIP-HOM purpose, which is (I suppose) to examine how close BP results are to Stokes results, should not come out any differently here, and thus it is not worth doing. Of course it is true that different numerical approaches generate different results in detail. But what exactly should the reader know about this numerical comparison? Can this be summarized in a sentence or two?

**I have shortened this section considerably, keeping the figures and only a minimum amount of text to describe them.**

lines 778-780: For efficiency I assume that BP is first used everywhere, then some criteria is applied, and then Stokes is used where the criteria applies. But do you want to demonstrate that the Stokes calculation everywhere gives the nearly same criteria-satisfying region?

I think this is done visually in Fig. 8. It is quite obvious that the Adaptive (AH) and Stokes (TS) calculations are quite close while the Blatter-Pattyn calculation is not very accurate in the details up through the column in the vicinity of the obstacle.

line 785: Is the "counterintuitive" aspect of this explained by noting that the effective viscosity is often actually largest in the top of the ice column, which implies the greatest longitudinal and bridging stress transmission up there? I often find that visualizing the effective viscosity, in these shear-thinning flows, illuminates where stresses de-localize the problem.

It is counterintuitive because I would have expected the Stokes calculation to be needed just in the vicinity of the obstacle and not far away at the top of the domain. Your explanation is probably correct but it would need a more detailed analysis to verify than is justified in this paper.

line 811-813: It is not the personal computer etc. which stops an analysis of the cost savings, but rather the lack of a performance model for the solver. This could be added, but it requires a bit of thinking.

Yes, but a more realistic calculation on representative computer hardware would be able to provide believable information on cost savings.

Subsection 6.2 and Section 7: This seems like tedious overkill. If a reader gets the main points of the paper then they can probably imagine lagging the Newton iteration and/or dual grids and/or higher order. In any case, another 300 lines are burned before the summary. If these are important enough then they could be a separate paper? Otherwise most readers won't have the endurance; really I don't.

In introducing the new transformation I stated that I wanted to bring out two of its applications (although there may be more): Adaptive switching and improved approximations that are more accurate than BP. I think both are equally important. Breaking it up into two papers is possible but it would lose some continuity. Honestly, I would not have the stamina to do that. Readers can always skip over parts that don't interest them.



Section 8 (Summary): Too long.

Substantially shortened.

Appendix A-C: On and on.

Appendix D: The manipulations shown in (79) and (80) are again very close to the main novel point of the paper. I see no reason why they can't be written into a new and prominent form which makes subsection 4.3.3 into the central material.

line 1521: Again, please don't say that all square matrices are invertible. (Literally the text says "the solvability condition  $[n_u=n_p]$  implies the invertibility of  $M_{\{WP\}}$ ". Just no.)

Appendices A and D eliminated. Material from Appendix D shortened and transferred to subsection 4.3.2. Sloppiness re matrix invertibility has been corrected.

# A Novel Transformation of the Ice Sheet Stokes Equations and Some of its Properties and Applications

John K. Dukowicz

Guest Scientist, Group T-3, Los Alamos National Laboratory,

Los Alamos, New Mexico, 87545, USA

*Correspondence to:* John K. Dukowicz (jn.dk@outlook.com)

**Abstract.** We introduce a novel transformation of the Stokes equations into a form that closely resembles the shallow Blatter-Pattyn equations. The two forms differ by only a few additional terms, while their variational formulations differ only by a single term in each horizontal direction. Specifically, the variational formulation of the Blatter-Pattyn model drops the vertical velocity in the second invariant of the strain rate tensor. Here we make use of the new transformation in two different ways. First, we consider incorporating the transformed equations into a code that can be very easily converted from a Stokes to a Blatter-Pattyn model, and vice-versa, by switching these terms on or off. This may be generalized so that the Stokes model is switched on adaptively only where the Blatter-Pattyn model loses accuracy. Second, the key role played by the vertical velocity in the Blatter-Pattyn approximation motivates new approximations that improve on the Blatter-Pattyn model. These applications require a grid that enables the discrete continuity equation to be invertible for the vertical velocity in terms of the horizontal velocity components. Examples of such grids, such as the first order P1-E0 grid and the second order P2-E1 grid are given in both 2D and 3D. It should be noted, however, that the transformed Stokes model has the same type of gravity forcing as the Blatter-Pattyn model, determined by the ice surface slope, thereby forgoing some of the grid-generality of the traditional formulation of the Stokes model.

## 1 Introduction

Concern and uncertainty about the magnitude of sea level rise due to melting of the Greenland and Antarctic ice sheets have led to increased interest in improved ice sheet and glacier modeling. The gold standard is a Stokes model (i.e., a model that solves the nonlinear, non-Newtonian Stokes system of equations for incompressible ice sheet dynamics) because it is applicable to all geometries and flow regimes. However, the Stokes model is computationally demanding and expensive to solve. It is a nonlinear, three-dimensional model involving four variables, namely, the three velocity components and pressure. In addition, pressure is a Lagrange multiplier enforcing incompressibility

38 and this creates a more difficult indefinite “saddle point” problem. As a result, full-  
39 Stokes models exist but are not commonly used in practice (examples are FELIX-S, Leng  
40 et al., 2012; Elmer/Ice, Gagliardini et al., 2013).

41

42 Because of these difficulties there is much interest in simpler and cheaper  
43 approximate models. There is a hierarchy of very simple models such as the shallow ice  
44 (SIA) and shallow-shelf (SSA) models, and there are also various **more accurate** higher-  
45 order approximations. These culminate in the Blatter-Pattyn (BP) approximation  
46 (Blatter, 1995; Pattyn, 2003), which is currently used in production code packages such  
47 as ISSM (Larour et al., 2012), MALI (Hoffman et al., 2018; Tezaur et al., 2015) and  
48 CISM (Lipscomb et al., 2019). This approximation is based on the assumption of a small  
49 ice sheet aspect ratio, i.e.,  $\varepsilon = H/L \ll 1$ , where  $H, L$  are the vertical and horizontal  
50 length scales, and consequently it eliminates certain stress terms and implicitly assumes  
51 small basal slopes. Both the Stokes and Blatter-Pattyn models are described in detail in  
52 Dukowicz et al. (2010), hereafter referred to as DPL (2010). Although the Blatter-Pattyn  
53 model is reasonably accurate for large-scale motions, accuracy deteriorates for small  
54 horizontal scales, less than about five ice thicknesses in the ISMIP–HOM model  
55 intercomparison (Pattyn et al., 2008; Perego et al., 2012), or below a 1 km resolution as  
56 found in a detailed comparison with full Stokes calculations (Rückamp et al., 2022). This  
57 can become particularly important for calculations involving details near the grounding  
58 line where the full accuracy of the Stokes model is needed (Nowicki and Wingham,  
59 2008). Attempts to address the problem while avoiding the use of full Stokes solvers  
60 include variable grid resolution coupled with a Blatter-Pattyn solver (Hoffman et al.,  
61 2018) and variable model complexity, where a Stokes solver is embedded locally in a  
62 lower order model (Seroussi et al., 2012). Better approximations, more accurate than  
63 Blatter-Pattyn but cheaper than Stokes, are currently not available.

64

65 The present paper introduces two innovations that may begin to address some of  
66 these issues. The first is a novel transformation of the Stokes model, described in §3,  
67 which puts it into a form closely resembling the Blatter-Pattyn model and differing only  
68 by the presence of a few extra terms. This allows a code to be switched over from Stokes  
69 to Blatter-Pattyn, and vice-versa, globally or locally, by the use of a single parameter that  
70 turns off these extra terms. As a result, variable model complexity can be very simply  
71 implemented, as described in §6.1. The second innovation is the introduction of new

72 finite element [discretizations](#) that decouple the discrete continuity equation and allow it to  
 73 be solved for the vertical velocity in terms of the horizontal velocity components.  
 74 Several elements used to construct such grids are described in Appendix C in both 2D  
 75 and 3D, primarily the first order P1-E0 and second order P2-E1 elements ([these two](#)  
 76 [elements are novel and are so-named because they employ pressures located on vertical](#)  
 77 [grid edges](#)). Within the framework of the transformed Stokes model these grids facilitate  
 78 new approximations that improve on the Blatter-Pattyn approximation so that it is no  
 79 longer strictly limited to a small ice sheet aspect ratio. We describe two such  
 80 approximations in §6.2. There is another very significant benefit. [An ice sheet Stokes](#)  
 81 [model is conventionally discretized as a constrained minimization problem requiring](#)  
 82 [special “stable” finite elements for solution. However, the same model on these new](#)  
 83 [grids can be formulated as an inherently stable and numerically equivalent unconstrained](#)  
 84 [minimization problem, as demonstrated in §4.3.2.](#)

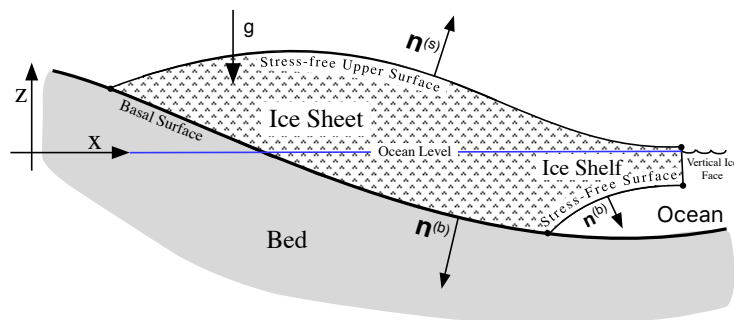
85

## 86 2 The Standard Formulation of the Stokes Ice Sheet Model

### 87 2.1 The Assumed Ice Sheet Configuration

88

89 An ice sheet may be divided into two parts, a part in contact with the bed and a floating  
 90 ice shelf located beyond the grounding line. The Stokes ice sheet model is capable of  
 91 describing the flow of an arbitrarily shaped ice sheet, including a floating ice shelf as  
 92 illustrated in Fig. 1, given appropriate boundary conditions (e.g., Cheng et al., 2020).  
 93 One limitation of the methods proposed here, in common with the Blatter-Pattyn model,  
 94 will be that there should [be just one upper and one basal surface](#), as is the case in Fig. 1.  
 95 Here we will only consider a fully grounded ice sheet with periodic lateral boundary  
 96 conditions, i.e., no ice shelf, [although in general ice shelves can be handled.](#)



97

98

99

**Figure 1** A simplified illustration of the admissible ice sheet configuration.

100

101 Referring to Fig. 1, the entire surface of the ice sheet is denoted by  $S$ . An upper  
 102 surface, labeled  $S_s$  and specified by  $\zeta_s(x, y, z) = z - z_s(x, y) = 0$ , is exposed to the  
 103 atmosphere and thus experiences stress-free boundary conditions. The bottom or basal  
 104 surface, denoted by  $S_B$  and specified by  $\zeta_b(x, y, z) = z - z_b(x, y) = 0$ , is in contact with  
 105 the bed. The basal surface may be subdivided into two sections,  $S_B = S_{B1} \cup S_{B2}$ , where  
 106  $S_{B1}$ , specified by  $z = z_{b1}(x, y)$ , is the part where ice is frozen to the bed (a no-slip  
 107 boundary condition), and  $S_{B2}$ , specified by  $z = z_{b2}(x, y)$ , is where frictional sliding  
 108 occurs. We assume Cartesian coordinates such that  $x_i = (x, y, z)$  are position coordinates  
 109 with  $z = 0$  at the ocean surface, and the index  $i \in \{x, y, z\}$  represents the three Cartesian  
 110 indices. Later we shall have occasion to introduce the restricted index  $(i) \in \{x, y\}$  to  
 111 represent just the two horizontal indices. [Note that this is equivalent to applying a](#)  
 112 [projection operator but is more compact, i.e.,  \$u\_{\(i\)} = P\_i\(u\) = \(u, v, 0\)\$ .](#) Unit normal vectors  
 113 appropriate for the ice sheet configuration of Fig. 1 are given by

$$\begin{aligned}
 n_i = (n_x, n_y, n_z) &= \frac{\partial \zeta_s(x, y, z) / \partial x_i}{|\partial \zeta_s(x, y, z) / \partial x_i|} = \frac{(-\partial z_s / \partial x, -\partial z_s / \partial y, 1)}{\sqrt{1 + (\partial z_s / \partial x)^2 + (\partial z_s / \partial y)^2}} && \text{at surface } S_s, \\
 n_i = (n_x, n_y, n_z) &= -\frac{\partial \zeta_b(x, y, z) / \partial x_i}{|\partial \zeta_b(x, y, z) / \partial x_i|} = \frac{(\partial z_b / \partial x, \partial z_b / \partial y, -1)}{\sqrt{1 + (\partial z_b / \partial x)^2 + (\partial z_b / \partial y)^2}} && \text{at surface } S_B.
 \end{aligned}
 \tag{1}$$

116

## 117 2.2 The Stokes Equations

118

119 The Stokes model is a system of nonlinear partial differential equations and associated  
 120 boundary conditions (Greve and Blatter, 2009; DPL, 2010). In a Cartesian coordinate  
 121 system the Stokes equations, the three momentum equations and the continuity equation,  
 122 for the three velocity components  $u_i = (u, v, w)$  and the pressure  $P$  are given by

$$\frac{\partial \tau_{ij}}{\partial x_j} - \frac{\partial P}{\partial x_i} + \rho g_i = 0, \tag{2}$$

123

124 
$$\frac{\partial u_i}{\partial x_i} = 0, \quad (3)$$

125 where  $\rho$  is the density, and  $g_i$  is the acceleration vector due to gravity, arbitrarily  
126 oriented in general but here taken to be in the negative z-direction,  $g_i = (0, 0, -g)$ .

127 Repeated indices imply summation (the Einstein notation). The deviatoric stress tensor  
128  $\tau_{ij}$  is given by

129 
$$\tau_{ij} = 2\mu_n \dot{\epsilon}_{ij}, \quad (4)$$

130 where the strain rate tensor is

131 
$$\dot{\epsilon}_{ij} = \frac{1}{2} \left( \frac{\partial u_i}{\partial x_j} + \frac{\partial u_j}{\partial x_i} \right), \quad (5)$$

132 the nonlinear ice viscosity  $\mu_n$  is a defined by

133 
$$\mu_n = \eta_0 (\dot{\epsilon}^2)^{(1-n)/2n}, \quad (6)$$

134 and  $\dot{\epsilon}^2 = \dot{\epsilon}_{ij} \dot{\epsilon}_{ij} / 2$  is the second invariant of the strain rate tensor that may be written out  
135 in full as follows

136 
$$\dot{\epsilon}^2 = \frac{1}{2} \left[ \left( \frac{\partial u}{\partial x} \right)^2 + \left( \frac{\partial v}{\partial y} \right)^2 + \left( \frac{\partial w}{\partial z} \right)^2 \right] + \frac{1}{4} \left[ \left( \frac{\partial u}{\partial y} + \frac{\partial v}{\partial x} \right)^2 + \left( \frac{\partial u}{\partial z} + \frac{\partial w}{\partial x} \right)^2 + \left( \frac{\partial v}{\partial z} + \frac{\partial w}{\partial y} \right)^2 \right]. \quad (7)$$

137 Note that the second invariant is a **positive quantity**, i.e.,  $\dot{\epsilon}^2 \geq 0$ . As usual, ice is assumed  
138 to obey Glen's flow law, where  $n$  is the Glen's law exponent ( $n = 1$  for a linear  
139 Newtonian fluid. Typically  $n = 3$  in ice sheet modeling, resulting in a nonlinear non-  
140 Newtonian fluid). The coefficient  $\eta_0$  is defined by  $\eta_0 = A^{-1/n} / 2$ , where  $A$  is an ice flow  
141 factor, here taken to be a constant but in general depending on temperature and other  
142 variables (see Schoof and Hewitt, 2013). The three-dimensional Stokes system requires a  
143 set of boundary conditions at every bounding surface, each set being composed of three  
144 components. Aside from the periodic lateral boundary conditions used in our test  
145 problems, the relevant boundary conditions are given as follows

146 (1) Stress-free boundary conditions on surfaces  $S_s$  not in contact with the bed, such  
147 as the upper surface  $S_s$  :

148 
$$\tau_{ij} n_j - P n_i = 0. \quad (8)$$

149 (2) No-slip or frozen to the bed conditions on surface segment  $S_{B1}$ :

$$150 \quad u_i = 0 \quad (9)$$

151 (3) Frictional tangential sliding conditions on surface segment  $S_{B2}$  in two parts:

152 (3a) A single condition enforcing tangential flow at the basal surface:

$$153 \quad u_i n_i = 0. \quad (10)$$

154 (3b) Two conditions specifying the horizontal components of the tangential  
155 frictional stress force vector, as follows

$$156 \quad \tau_{(i)j} n_j - \tau_n n_{(i)} + \tau_i^S = 0, \quad (11)$$

157 where  $\tau_n = n_i \tau_{ij} n_j$  is the normal component of the shear stress, and  $\tau_i^S$  is a specified  
158 interfacial shear stress, tangential to the bed ( $n_i \tau_i^S = 0$ ). The tangential shear stress or  
159 traction is obtained as in DPL (2010) by subtracting out the normal component from the  
160 shear stress. However, the three components of the tangential shear stress are not  
161 independent because they already satisfy the tangency condition at the basal surface and  
162 therefore we retain only the horizontal components. The interfacial shear stress  $\tau_i^S$  is  
163 potentially a complicated function of position and velocity (e.g., Schoof, 2010).  
164 However, here we assume only simple linear frictional sliding,

$$165 \quad \tau_i^S = \beta(x) u_i, \quad (12)$$

166 where  $\beta(x) > 0$  is a position-dependent drag law coefficient. For simplicity we assume  
167 there is no melting or refreezing at the bed resulting in vertical inflows or outflows. If  
168 needed, these can be easily added to (10) (Dukowicz et al., 2010; Heinlein et al., 2022).

169

### 170 **2.3 The Stokes Variational Principle**

171

172 A variational principle, if available, is usually the most compact way of representing a  
173 particular problem. The Stokes model possesses a variational principle that is  
174 particularly useful for discretization purposes and for the specification of boundary  
175 conditions (see DPL, 2010, and Chen et al., 2013, for a fuller description of the  
176 variational principle applied to ice sheet modeling). There are a number of significant  
177 advantages. For example, all boundary conditions are conveniently incorporated in the  
178 variational formulation, all terms in the variational functional, including boundary  
179 condition terms, contain lower order derivatives than in the momentum equations, and the

180 resulting discretization automatically involves a symmetric matrix. In discretizing the  
 181 momentum equations, stress terms at boundaries involve derivatives **that would normally**  
 182 **have to be evaluated using less accurate one-sided approximations**. This problem does  
 183 not arise in the variational formulation since all terms are evaluated in the interior.  
 184 Finally, stress-free boundary conditions, as at the upper surface for example, need not be  
 185 specified at all since they are automatically incorporated in the functional as natural  
 186 boundary conditions. In discrete applications, the variational method presented here is  
 187 closely related to the Galerkin finite element method, a subset of the weak formulation  
 188 method in which the test and trial functions are the same (see Schoof, 2010, **and earlier**  
 189 **references contained therein** in connection with the Blatter-Pattyn model).

190

191 The variational functional for the standard Stokes model may be written in two  
 192 alternative forms:

193 (1) Basal boundary conditions imposed using Lagrange multipliers:

$$194 \quad \mathcal{A}[u_i, P, \lambda_i, \Lambda] = \int_V dV \left[ \frac{4n}{n+1} \eta_0 (\dot{\epsilon}^2)^{(1+n)/2n} - P \frac{\partial u_i}{\partial x_i} + \rho g w \right] \quad (13)$$

$$+ \int_{S_{B1}} dS \lambda_i u_i + \int_{S_{B2}} dS \left[ \Lambda u_i n_i + \frac{1}{2} \beta(x) u_i u_i \right],$$

195 where  $\lambda_i$  and  $\Lambda$  are Lagrange multipliers used to enforce the no-slip condition and  
 196 frictional tangential sliding, respectively. As in DPL (2010), arguments enclosed in  
 197 square brackets, here  $u_i, P, \lambda_i, \Lambda$ , **indicates those functions that are subject to variation as**  
 198 **arguments of the functional**.

199 (2) Basal boundary conditions imposed by direct substitution:

200 In this case, the two conditions (9), (10) are used directly in the functional to specify all  
 201 three velocity components  $u_i$  in the first case, and the vertical velocity  $w$  in terms of the  
 202 horizontal velocity components in the second case, along the entire basal boundary in  
 203 both the volume and surface integrals in (13). **However, this can only be done in the**  
 204 **discrete formulation of the functional since only then are boundary values of velocity**  
 205 **accessible (except in the surface integral terms where they are always accessible)**. In  
 206 particular, the tangential flow condition (10) is used in the following form,

$$207 \quad w = -\frac{u_{(i)} n_{(i)}}{n_z} = u_{(i)} \frac{\partial z_b}{\partial x_{(i)}}, \quad (14)$$

208 to eliminate  $w$  on the basal boundary segment  $S_{B2}$  of the variational functional, to obtain



$$\begin{aligned}
209 \quad \mathcal{A}[u_i, P] = & \int_V dV \left[ \frac{4n}{n+1} \eta_0 (\dot{\epsilon}^2)^{(1+n)/2n} - P \frac{\partial u_i}{\partial x_i} + \rho g w \right] \\
& + \frac{1}{2} \int_{S_{B2}} dS \beta(x) \left( u_{(i)} u_{(i)} + \left( u_{(i)} n_{(i)} / n_z^{(b2)} \right)^2 \right).
\end{aligned} \tag{15}$$

210 It is important to emphasize again that boundary conditions (9) and (14) must also be  
211 applied in the volume integral part of the discretized functional (15) as part of direct  
212 substitution to replace velocity variables that lie on the basal boundary. In the case of  
213 (14), horizontal velocity variables remain undisturbed while  $w$  is eliminated, thus  
214 implementing the tangential sliding boundary condition.

215  
216 As described in DPL (2010), a variational procedure yields the full set of Euler-  
217 Lagrange equations and boundary conditions that specify the standard Stokes model,  
218 equivalent to (2)-(11). In the case of (13), the system determines all the discrete variables  
219 specified on the mesh: the velocity components and the pressure,  $u_i, P$ , as well as the  
220 Lagrange multipliers,  $\lambda_j, \Lambda$ . In the direct substitution case, (15), the numerical solution  
221 determines only the pressure  $P$  and those velocity variables  $u_i$  that were not directly  
222 prescribed as boundary conditions in (9) or (14). These prescribed (known) values of  
223 boundary velocities are then added a posteriori. As a result, the direct substitution  
224 method is smaller and simpler, and therefore is the one primarily used in the paper.

225

### 226 3. A Transformation of the Stokes Model

#### 227 3.1 Origin of the Transformation

228

229 The transformation is motivated by the Blatter-Pattyn approximation. Consider the  
230 vertical component of the momentum equation and the corresponding stress-free upper  
231 surface boundary condition in the Blatter-Pattyn approximation (from DPL, 2010, for  
232 example), which are given by

$$\begin{aligned}
233 \quad \frac{\partial}{\partial z} \left( 2\mu_n \frac{\partial w}{\partial z} \right) - \frac{\partial P}{\partial z} - \rho g &= 0, \\
\left( 2\mu_n \frac{\partial w}{\partial z} - P \right) n_z &= 0 \quad \text{at } z = z_s(x, y).
\end{aligned} \tag{16}$$

234 These equations may be rewritten in the form

235 
$$\frac{\partial}{\partial z} \left( P - 2\mu_n \frac{\partial w}{\partial z} + \rho g(z - z_s(x, y)) \right) = 0, \quad (17)$$

236 
$$\left( P - 2\mu_n \frac{\partial w}{\partial z} + \rho g(z - z_s(x, y)) \right) n_z = 0 \quad \text{at} \quad z = z_s(x, y),$$

236 suggesting a new variable  $\tilde{P}$ , to be called the transformed pressure, as follows

237 
$$\tilde{P} = P - 2\mu_n \frac{\partial w}{\partial z} + \rho g(z - z_s(x, y)), \quad (18)$$

238 which simplifies system (17) to give

239 
$$\frac{\partial \tilde{P}}{\partial z} = 0, \quad (19)$$

240 
$$\tilde{P} n_z = 0 \quad \text{at} \quad z = z_s(x, y).$$

240 This is a complete one-dimensional partial differential system, that, when integrated from  
241 the top surface down yields

242 
$$\tilde{P} = 0. \quad (20)$$

243 Thus, the transformed pressure vanishes in the Blatter-Pattyn case. The definition (18)  
244 forms the basis of the present transformation but we also use the continuity equation to  
245 eliminate  $\partial w / \partial z$  as is done in the Blatter-Pattyn approximation (e.g., Pattyn, 2003).

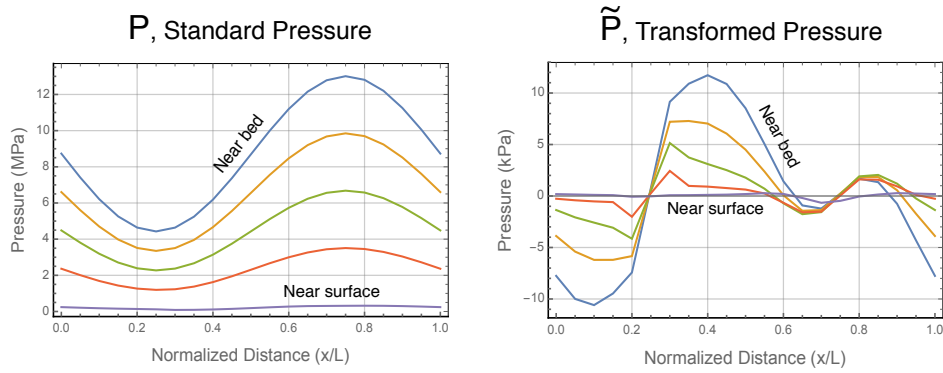
246 Therefore, the transformation consists of eliminating  $P$  and  $\partial w / \partial z$  in the Stokes system  
247 (2), (4)-(11) (i.e., everywhere except in the continuity equation (3) itself) by means of

248 
$$P = \tilde{P} - 2\mu_n \left( \frac{\partial u}{\partial x} + \frac{\partial v}{\partial y} \right) + \rho g(z_s - z), \quad (21)$$

249 
$$\frac{\partial w}{\partial z} = - \left( \frac{\partial u}{\partial x} + \frac{\partial v}{\partial y} \right). \quad (22)$$

250

251 The pressure  $P$  in the standard Stokes system is primarily a Lagrange multiplier  
252 enforcing incompressibility, but with a very large hydrostatic component. The  
253 transformation eliminates the hydrostatic pressure from  $\tilde{P}$ , as illustrated in Fig. 2 where  
254 the two pressures are compared. **The transformed pressure  $\tilde{P}$  is some three orders of**  
255 **magnitude smaller than the standard Stokes pressure  $P$  primarily because of the absence**  
256 **of hydrostatic pressure.**



257

258 **Figure 2.** Standard pressure  $P$  compared to the transformed pressure  $\tilde{P}$  in Exp. B from  
 259 the ISMIP–HOM model intercomparison (Pattyn et al., 2008) at  $L = 10$  km.

260

Note that  $P$  is in MPa while  $\tilde{P}$  is in kPa.

261

262 The transformed pressure  $\tilde{P}$  is again a Lagrange multiplier enforcing  
 263 incompressibility. Alternatively, since  $\tilde{P} = 0$  in the Blatter-Pattyn approximation, the  
 264 transformed pressure may be written as  $\tilde{P} = P - P_{BP}$ , where

265

$$P_{BP} = -2\mu_n \left( \frac{\partial u}{\partial x} + \frac{\partial v}{\partial y} \right) + \rho g (z_s - z)$$

266 is the effective Blatter-Pattyn pressure (Tezaur et al., 2015). As a result,  $P = P_{BP} + \tilde{P}$  and

267 therefore  $\tilde{P}$  is actually the ‘‘Stokes’’ correction to the Blatter-Pattyn pressure.

268

### 269 3.2 The Transformed Stokes Equations

270

271 Introducing (21), (22) into the Stokes system of equations (2)-(11) results in the  
 272 following transformed Stokes system:

$$273 \quad \frac{\partial \tilde{\tau}_{ij}}{\partial x_j} - \hat{\xi} \frac{\partial \tilde{P}}{\partial x_i} - \rho g \frac{\partial z_s}{\partial x_{(i)}} = 0, \quad (23)$$

$$274 \quad \hat{\xi} \frac{\partial u_i}{\partial x_i} = 0, \quad (24)$$

275 where quantities that are modified in the transformation are indicated by a tilde, e.g.,  $\tilde{P}$ .

276 Here and in the following we will be using dummy variables  $\xi, \hat{\xi}$  to indicate terms that

277 are absent in the Blatter-Blatter approximation, as explained below. Corresponding to (4)  
 278 the modified Stokes deviatoric stress tensor  $\tilde{\tau}_{ij}$  is given by

$$279 \quad \tilde{\tau}_{ij} = 2\tilde{\mu}_n \left( \tilde{\epsilon}_{ij} + \frac{\partial u_{(i)}}{\partial x_{(j)}} \delta_{ij} \right), \quad (25)$$

280 where  $\delta_{ij}$  is the Kronecker delta, the modified strain rate tensor  $\tilde{\epsilon}_{ij}$ , corresponding to (5),  
 281 is given by

$$282 \quad \tilde{\epsilon}_{ij} = \begin{bmatrix} \frac{\partial u}{\partial x} & \frac{1}{2} \left( \frac{\partial u}{\partial y} + \frac{\partial v}{\partial x} \right) & \frac{1}{2} \left( \frac{\partial u}{\partial z} + \xi \frac{\partial w}{\partial x} \right) \\ \frac{1}{2} \left( \frac{\partial u}{\partial y} + \frac{\partial v}{\partial x} \right) & \frac{\partial v}{\partial y} & \frac{1}{2} \left( \frac{\partial v}{\partial z} + \xi \frac{\partial w}{\partial y} \right) \\ \frac{1}{2} \left( \frac{\partial u}{\partial z} + \xi \frac{\partial w}{\partial x} \right) & \frac{1}{2} \left( \frac{\partial v}{\partial z} + \xi \frac{\partial w}{\partial y} \right) & - \left( \frac{\partial u}{\partial x} + \frac{\partial v}{\partial y} \right) \end{bmatrix} \quad (26)$$

283 and, corresponding to (6), the modified viscosity,

$$284 \quad \tilde{\mu}_n = \eta_0 \left( \tilde{\epsilon}^2 \right)^{(1-n)/2n}, \quad (27)$$

285 is given in terms of the second invariant,  $\tilde{\epsilon}^2 = \tilde{\epsilon}_{ij} \tilde{\epsilon}_{ij} / 2$ , that in expanded form becomes

$$286 \quad \tilde{\epsilon}^2 = \left( \frac{\partial u}{\partial x} \right)^2 + \frac{\partial u}{\partial x} \frac{\partial v}{\partial y} + \left( \frac{\partial v}{\partial y} \right)^2 + \frac{1}{4} \left[ \left( \frac{\partial u}{\partial y} + \frac{\partial v}{\partial x} \right)^2 + \left( \frac{\partial u}{\partial z} + \xi \frac{\partial w}{\partial x} \right)^2 + \left( \frac{\partial v}{\partial z} + \xi \frac{\partial w}{\partial y} \right)^2 \right]. \quad (28)$$

287 Since (28) differs from (7) only by the use of the continuity equation (22), the

288 transformation will leave the second invariant  $\tilde{\epsilon}^2$  and viscosity  $\tilde{\mu}_n$  unchanged, i.e.,

289  $\tilde{\epsilon}^2 = \epsilon^2$  and  $\tilde{\mu}_n = \mu_n$ , and the transformed second invariant remains positive, i.e.,  $\tilde{\epsilon}^2 \geq 0$ .

290

291 The dummy variables  $\xi, \hat{\xi}$  in (23)-(25) and (26)-(29) are used to identify terms  
 292 that are neglected in the two types of the Blatter-Pattyn approximation discussed in §3.4.

293 These are (a) the standard Blatter-Pattyn approximation,  $\xi = 0, \hat{\xi} = 0$ , as originally

294 derived (Blatter, 1995; Pattyn, 2003; DPL, 2010), which solves for just the horizontal

295 velocity components  $u, v$ , and (b) the extended Blatter-Pattyn approximation,

296  $\xi = 0, \hat{\xi} = 1$ , described more fully later, that contains the standard approximation and also

297 contains additional equations that determine the vertical velocity  $w$  and the pressure  $\tilde{P}$ .

298 Keeping all terms, i.e.,  $\xi = 1, \hat{\xi} = 1$ , specifies the full transformed Stokes model.

299

300 Boundary conditions for the transformed equations, corresponding to (8)-(11), are  
301 given by

302 BCs on  $S_S$  : 
$$\tilde{\tau}_{ij} n_j - \hat{\xi} \tilde{P} n_i = 0 , \quad (29)$$

303 BCs on  $S_{B1}$  : 
$$u_i = 0 , \quad (30)$$

304 BCs on  $S_{B2}$  : 
$$u_i n_i = 0 , \quad (31)$$

305 
$$\tilde{\tau}_{(i)j} n_j - \tilde{\tau}_n n_{(i)} + \beta(x) u_{(i)} = 0 , \quad (32)$$

306 where  $\tilde{\tau}_n = n_i \tilde{\tau}_{ij} n_j$  as before. Equations (31), (32) constitute the three required boundary  
307 conditions for frictional sliding.

308

309 The transformed system, (25)-(32), and the standard Stokes system, (2)-(11), yield  
310 exactly the same solution. However, in common with the Blatter-Pattyn approximation,  
311 transformation (21) **needs to use** a gravity-oriented coordinate system because of the  
312 particular form of the gravitational forcing term, while the standard Stokes model does  
313 not have this restriction. This is not a major limitation. A somewhat more restrictive  
314 limitation is the appearance of  $z_s(x, y)$ , an implicitly single valued function, to describe  
315 the vertical position of the upper surface of the ice sheet. This means that care must be  
316 taken in case of reentrant upper surfaces (i.e., S-shaped in 2D) and sloping cliffs at the ice  
317 edge, a restriction not present in the standard Stokes model. For simplicity, as noted  
318 before we assume that there is **just one upper and one basal surface, i.e., as is usual in ice**  
319 **sheet modeling we do not permit overhangs.**

320

### 321 **3.3 The Transformed Stokes Variational Principle**

322

323 It is easy to verify that the transformed Stokes system (23)-(32) results from the variation  
324 with respect to  $u_i, \tilde{P}$  of the following functional:

$$\begin{aligned}
325 \quad \tilde{\mathcal{A}}[u_i, \tilde{P}] = & \int_V dV \left[ \frac{4n}{n+1} \eta_0 (\tilde{\epsilon}^2)^{(1+n)/2n} - \hat{\xi} \tilde{P} \frac{\partial u_i}{\partial x_i} + \rho g u_{(i)} \frac{\partial z_s}{\partial x_{(i)}} \right] \\
& + \frac{1}{2} \int_{S_{B2}} dS \beta(x) \left( u_{(i)} u_{(i)} + \left( u_{(i)} n_{(i)} / n_z \right)^2 \right), \quad (33)
\end{aligned}$$

326 where  $\tilde{\epsilon}^2$  is the transformed second invariant from (28). Basal boundary conditions are  
327 imposed by direct substitution, as in (15). Alternatively, one could also impose boundary  
328 conditions using Lagrange multipliers as in (13), **if desired**.

329

### 330 **3.4 Two Blatter-Pattyn Approximations**

#### 331 **3.4.1 The Standard Blatter-Pattyn Approximation**

332

333 The standard (or traditional) Blatter-Pattyn approximation (originally introduced by  
334 Blatter, 1995; Pattyn, 2003; later by DPL, 2010; Schoof and Hewitt, 2013, **and references**  
335 **therein**) is obtained by setting  $\xi = 0$ ,  $\hat{\xi} = 0$  in the transformed system. This yields the  
336 following Blatter-Pattyn variational functional,

$$\begin{aligned}
337 \quad \mathcal{A}_{BP}[u_{(i)}] = & \int_V dV \left[ \frac{4n}{n+1} \eta_0 (\dot{\epsilon}_{BP}^2)^{(1+n)/2n} + \rho g u_{(i)} \frac{\partial z_s}{\partial x_{(i)}} \right] \\
& + \frac{1}{2} \int_{S_{B2}} dS \beta(x) \left( u_{(i)} u_{(i)} + \zeta \left( u_{(i)} n_{(i)} / n_z \right)^2 \right), \quad (34)
\end{aligned}$$

338 in terms of horizontal velocity components only, where **the second invariant**  $\dot{\epsilon}_{BP}^2$  **follows**  
339 **from (28) with**  $\xi = 0$ ,

$$340 \quad \dot{\epsilon}_{BP}^2 = \left( \frac{\partial u}{\partial x} \right)^2 + \frac{\partial u}{\partial x} \frac{\partial v}{\partial y} + \left( \frac{\partial v}{\partial y} \right)^2 + \frac{1}{4} \left[ \left( \frac{\partial u}{\partial y} + \frac{\partial v}{\partial x} \right)^2 + \frac{\partial u^2}{\partial z} + \frac{\partial v^2}{\partial z} \right], \quad (35)$$

341 and therefore the Euler-Lagrange equations and boundary conditions become

$$342 \quad \frac{\partial \tau_{(i)j}^{BP}}{\partial x_j} - \rho g \frac{\partial z_s}{\partial x_{(i)}} = 0; \quad \begin{cases} \tau_{(i)j}^{BP} n_j + \beta(x) \left( u_{(i)} + \zeta \left( u_{(j)} n_{(j)} / n_z \right) n_{(i)} / n_z \right) = 0 \\ \text{on } S_{B2}, \quad \tau_{(i)j}^{BP} n_j = 0 \text{ on } S_S, \quad u_{(i)} = 0 \text{ on } S_{B1}, \end{cases} \quad (36)$$

343 where the Blatter-Pattyn stress tensor  $\tau_{(i)j}^{BP}$  is

$$344 \quad \tau_{(ij)}^{BP} = \eta_0 \left( \dot{\epsilon}_{BP}^2 \right)^{(1-n)/2n} \begin{bmatrix} 2 \left( 2 \frac{\partial u}{\partial x} + \frac{\partial v}{\partial y} \right) & \left( \frac{\partial u}{\partial y} + \frac{\partial v}{\partial x} \right) & \frac{\partial u}{\partial z} \\ \left( \frac{\partial u}{\partial y} + \frac{\partial v}{\partial x} \right) & 2 \left( \frac{\partial u}{\partial x} + 2 \frac{\partial v}{\partial y} \right) & \frac{\partial v}{\partial z} \end{bmatrix}. \quad (37)$$

345 **These last two equations correspond to (23) and (25) in the transformed Stokes system.**  
 346 There is a new dummy variable  $\zeta$  in (34) introduced to identify the basal boundary term  
 347 normally dropped ( $\zeta = 0$ ) in the standard Blatter-Pattyn approximation but restored  
 348 ( $\zeta = 1$ ) in Dukowicz et al. (2011) to better deal with arbitrary basal topography.

349

350 The Blatter-Pattyn model is a well-behaved nonlinear approximate system for the  
 351 horizontal velocity components  $u, v$  because in this case the variational formulation is a  
 352 convex optimization problem whose solution minimizes the functional. As noted in the  
 353 Introduction, the Blatter-Pattyn approximation is widely used in practice as an  
 354 economical and relatively accurate ice sheet model. If desired, the vertical velocity  
 355 component  $w$  may be computed a posteriori by means of the continuity equation.

356

357 **Remark #1:** The original formulation (e.g., Pattyn, 2003) approximates the normal unit  
 358 vectors  $n_i$  on the frictional part of the basal boundary  $S_{B2}$  by making the small slope  
 359 approximation. However, this additional approximation is unnecessary since any  
 360 computational savings are negligible (Dukowicz et al., 2011; Perego et al., 2012).

361

### 362 **3.4.2 The Extended Blatter-Pattyn Approximation**

363

364 A second form of the Blatter-Pattyn approximation is obtained from the transformed  
 365 variational principle (33) by making the assumption,

$$366 \quad \left\| \frac{\partial w}{\partial x} \right\| \ll \left\| \frac{\partial u}{\partial z} \right\|, \quad \left\| \frac{\partial w}{\partial y} \right\| \ll \left\| \frac{\partial v}{\partial z} \right\|, \quad (38)$$

367 and therefore neglecting  $\partial w / \partial x, \partial w / \partial y$  in the transformed second invariant  $\tilde{\epsilon}^2$ , or  
 368 equivalently, in the strain rate tensor  $\tilde{\epsilon}_{ij}$  from (26), consistent with the original small  
 369 aspect ratio approximation (Blatter, 1995; Pattyn, 2003; DPL, 2010; Schoof and  
 370 Hindmarsh, 2008). This corresponds to setting  $\xi = 0, \hat{\xi} = 1$  in the transformed Stokes  
 371 model. In other words, we neglect vertical velocity gradients but keep the pressure term.

372 This will be called the extended Blatter-Pattyn approximation (EBP) because, in contrast  
 373 to the standard Blatter-Pattyn approximation, all the variables, i.e.,  $u, v, w, \tilde{P}$ , are retained.  
 374 Notably, assumption (38) is equivalent to just setting  $w = 0$  in the second invariant  $\tilde{\epsilon}^2$  in  
 375 the full transformed Stokes model. That is, the extended BP approximation is obtained  
 376 by neglecting vertical velocities everywhere in (33) except where they occurs in the  
 377 velocity divergence term. This aspect of the transformed Stokes model will be exploited  
 378 later to obtain approximations that improve on Blatter-Pattyn. Thus, the extended  
 379 Blatter-Pattyn functional is given by

$$380 \quad \mathcal{A}_{EBP}[u_i, \tilde{P}] = \int_V dV \left[ \frac{4n}{n+1} \eta_0 (\dot{\epsilon}_{BP}^2)^{(1+n)/2n} - \tilde{P} \frac{\partial u_i}{\partial x_i} + \rho g u_{(i)} \frac{\partial z_s}{\partial x_{(i)}} \right] \\
 + \frac{1}{2} \int_{S_{B2}} dS \beta(x) \left( u_{(i)} u_{(i)} + \zeta \left( u_{(i)} n_{(i)} / n_z \right)^2 \right), \quad (39)$$

381 and the Blatter-Pattyn second invariant  $\dot{\epsilon}_{BP}^2$  is given by (35). Taking the variation of the  
 382 functional, the system of extended Blatter-Pattyn Euler-Lagrange equations and their  
 383 boundary conditions is given by

384 (1) Variation with respect to  $u_{(i)}$  yields the horizontal momentum equation:

$$385 \quad \frac{\partial \tau_{(i)j}^{BP}}{\partial x_j} - \frac{\partial \tilde{P}}{\partial x_{(i)}} - \rho g \frac{\partial z_s}{\partial x_{(i)}} = 0; \quad \begin{cases} \tau_{(i)j}^{BP} n_j - \tilde{P} n_{(i)} = 0 \text{ on } S_S, & u_{(i)} = 0 \text{ on } S_{B1}, \\ \tau_{(i)j}^{BP} n_j + \beta(x) \left( u_{(i)} + \zeta \left( u_{(k)} n_{(k)} / n_z \right) n_{(i)} / n_z \right) = 0 \\ \text{on } S_{B2}, \end{cases} \quad (40)$$

386 where  $\tau_{(i)j}^{BP}$  is given by (37).

387 (2) Variation with respect to  $w$  yields the vertical momentum equation:

$$388 \quad -\frac{\partial \tilde{P}}{\partial z} = 0; \quad \tilde{P} n_z = 0 \text{ on } S_S, \quad (41)$$

389 (3) Variation with respect to  $\tilde{P}$  yields the continuity equation:

$$390 \quad \frac{\partial w}{\partial z} + \frac{\partial u_{(i)}}{\partial x_{(i)}} = 0; \quad w = 0 \text{ on } S_{B1}, \text{ or } w = -u_{(i)} n_{(i)} / n_z \text{ on } S_{B2}. \quad (42)$$

391 It is apparent that the vertical momentum equation system (41) is decoupled, yielding  
 392  $\tilde{P} = 0$ , as was already shown in §3.1. This eliminates pressure from the horizontal  
 393 momentum equation (40), making it a decoupled equation for the horizontal velocities



394  $u_{(i)}$ , identical to the standard Blatter-Pattyn system (36). In addition, having obtained the  
 395 horizontal velocities from (40), the continuity equation (42) may now be solved for the  
 396 vertical velocity  $w$  (but see the comments regarding the discrete case that follow (43)).  
 397

398 In summary, the extended Blatter-Pattyn model, (40)-(42), is equivalent to the  
 399 standard Blatter-Pattyn model, (36), for the horizontal velocities,  $u, v$ , except that it also  
 400 includes two additional equations that determine the pressure  $\tilde{P}$  and the vertical velocity  
 401  $w$  that are usually ignored in the standard Blatter-Pattyn approximation where only the  
 402 horizontal velocity is calculated. Because of this, we distinguish between the *Blatter-*  
 403 *Pattyn model* that solves for just the two horizontal velocities (i.e., the standard Blatter-  
 404 Pattyn approximation, (36)), and the *Blatter-Pattyn system* that solves for all the variables  
 405 (i.e., the extended Blatter-Pattyn approximation, (40)-(42)). *Perhaps the main distinction*  
 406 *between the two, which may be important in some applications, is that the Blatter-Pattyn*  
 407 *system obtains the vertical velocity on the same grid as the horizontal velocities, while in*  
 408 *the Blatter-Pattyn model the calculation of vertical velocity is completely decoupled and*  
 409 *may be done on an unrelated grid. These models must obtain the vertical velocity  $w$*   
 410 *from the continuity equation (42) once horizontal velocities  $u, v$  are available. In the*  
 411 *continuous case this can be done using the Leibniz's theorem, as follows*

$$412 \quad w(u, v) = w_{z=z_b} - \int_{z_b}^z \frac{\partial u_{(i)}}{\partial x_{(i)}} dz' = u_{(i)} \frac{\partial z_b}{\partial x_{(i)}} - \int_{z_b}^z \frac{\partial u_{(i)}}{\partial x_{(i)}} dz' = -\frac{\partial}{\partial x_{(i)}} \int_{z_b}^z u_{(i)} dz' . \quad (43)$$

413 *In the discrete case one may consider discretizing (43) directly. However, later we*  
 414 *consider special finite element grids where the continuity equation is stably solved for  $w$ .*  
 415

416 So far we have only considered continuum properties of Stokes-type systems.  
 417 However, a discrete finite element formulation may not be well behaved. The solution of  
 418 discretized Stokes models and Blatter-Pattyn approximations, and the solution for vertical  
 419 velocity from the continuity equation will depend on the choices made for the grids and  
 420 the finite elements that are to be used. These issues will be discussed next.

421

## 422 **4. Finite Element Discretization**

### 423 **4.1 Standard and Transformed Stokes Discretizations**

424

425 In practice, both traditional Stokes and Blatter-Pattyn models are discretized using finite  
 426 element methods (e.g., Gagliardini et al., 2013; Perego et al., 2012). We follow this

427 practice except that here the discretization originates from a variational principle. This  
 428 has a number of advantages (see §2.3 and DPL, 2010). The following is a brief outline of  
 429 the finite element discretization. Additional details about the grid and the associated  
 430 discretization are provided in Appendix B. For simplicity, we confine ourselves to two  
 431 dimensions with coordinates  $(x, z)$  and velocities  $(u, w)$ . Generalization to three  
 432 dimensions is possible (an example of a three-dimensional grid appropriate for our  
 433 purpose is discussed in Appendix B). Further, we discuss only the case of direct  
 434 substitution for basal boundary conditions in the variational functional, i.e., (15) or (33).  
 435 The remarks in this Section will apply to both the standard and transformed Stokes  
 436 models; for example, the discrete pressure variable  $p$  may refer to either the standard  
 437 pressure  $P$  or the transformed pressure  $\tilde{P}$ .

438

439 Consider an arbitrary grid with a total of  $N = n_u + n_w + n_p$  unknown discrete  
 440 variables at appropriate nodal locations  $1 \leq i \leq N$ , with  $n_u$  horizontal velocity variables,  
 441  $n_w$  vertical velocity variables, and  $n_p$  pressure variables, so that

$$442 \quad V = \{V_1, V_2, \dots, V_N\}^T = \left\{ \left\{ u_1, u_2, \dots, u_{n_u} \right\}, \left\{ w_1, w_2, \dots, w_{n_w} \right\}, \left\{ p_1, p_2, \dots, p_{n_p} \right\} \right\}^T = \{u, w, p\}^T \quad (44)$$

443 is the vector of all the unknown discrete variables that are the degrees of freedom of the  
 444 model. If using Lagrange multipliers for basal boundary conditions then discrete  
 445 variables corresponding to  $\lambda_z, \Lambda$  must be added. Variables are expanded in terms of  
 446 shape functions  $N_i^k(\mathbf{x})$  associated with each nodal variable  $i$  in each element  $k$ , so that

$$447 \quad V^k(\mathbf{x}) = \sum_i V_i N_i^k(\mathbf{x})$$

is the spatial variation of all variables in element  $k$ , summed over

448 all variable nodes located in element  $k$ . Shape functions associated with a given node  
 449 may differ depending on the variable (i.e.,  $u, w$ , or  $p$ ). Substituting into the functional,  
 450 (15) or (33), integrating and assembling the contributions of all elements, we obtain a  
 451 discretized variational functional in terms of the nodal variable vectors  $u, w, p$ , as follows

$$452 \quad \mathcal{A}(u, w, p) = \sum_k \mathcal{A}^k(u, w, p), \quad (45)$$

453 where  $\mathcal{A}^k(u, w, p)$  is the local functional evaluated by integrating over element  $k$ . Since  
 454 the term in the functional involving the product of pressure and divergence of velocity is

455 linear in pressure and velocity, and the term responsible for gravity forcing is linear in  
456 velocity, the functional (45) may be written in matrix form as follows

$$457 \quad \mathcal{A}(u, w, p) = \mathcal{M}(u, w) + p^T (M_{UP}^T u + M_{WP}^T w) + u^T F_U + w^T F_W, \quad (46)$$

458 where the notation from (44) has been used, i.e.,  $u = \{u_1, u_2, \dots, u_{n_u}\}^T$ , etc. Parentheses  
459 indicate a functional dependence on the indicated variables. Comparison with (15) and  
460 (33) indicates that  $\mathcal{M}(u, w)$  is a nonlinear positive-definite function of the velocity  
461 components  $u, w$ ,  $M_{UP}^T, M_{WP}^T$  are constant  $n_p \times n_u$  and  $n_p \times n_w$  matrices, respectively,  
462 arising from the incompressibility constraint, and  $F_U, F_W$  are constant gravity forcing  
463 vectors, of dimension  $n_u$  and  $n_w$ , respectively. Note that  $F_U = 0, F_W \neq 0$  specifies the  
464 standard Stokes model, and  $F_U \neq 0, F_W = 0$  the transformed Stokes model. The discrete  
465 functional  $\mathcal{M}(u, w)$  differs but it remains positive-definite in both.

466

467 Discrete variation of the functional corresponds to partial differentiation with  
468 respect to each of the discrete variables in  $V$ . Thus, the discrete Euler-Lagrange  
469 equations that correspond to the **u-momentum**, **w-momentum**, and continuity equations,  
470 respectively, are given by

$$471 \quad R(u, w, p) = \begin{bmatrix} R_U(u, w, p) \\ R_W(u, w, p) \\ R_p(u, w) \end{bmatrix} = \begin{bmatrix} \mathcal{M}_U(u, w) + M_{UP} p + F_U \\ \mathcal{M}_W(u, w) + M_{WP} p + F_W \\ M_{UP}^T u + M_{WP}^T w \end{bmatrix} = 0, \quad (47)$$

472 where  $R(u, w, p)$  is the residual vector with components  $R_U(u, w, p) = \partial \mathcal{A} / \partial u$ ,

473  $R_W(u, w, p) = \partial \mathcal{A} / \partial w$ , and  $R_p(u, w) = \partial \mathcal{A} / \partial p$ . The functionals  $\mathcal{M}_U(u, w) = \partial \mathcal{M} / \partial u$ ,

474  $\mathcal{M}_W(u, w) = \partial \mathcal{M} / \partial w$  are nonlinear vectors of dimension  $n_u$  and  $n_w$ , respectively.

475 Altogether, (47) is a set of  $N$  equations for the  $N$  unknown discrete variables  $V_i$ . As  
476 explained previously, all boundary conditions are already included in functional (46), and  
477 therefore are also incorporated into the discrete Euler-Lagrange equations (47).

478

479 Since the overall system (47) is nonlinear, it is typically solved using Newton-  
480 Raphson iteration, expressed in matrix notation as follows

481 
$$M(u^K, w^K) \Delta V + R(u^K, w^K, p^K) = 0, \quad (48)$$

482 where  $K$  is the iteration index,  $M(u, v) = \partial^2 \mathcal{A}(V) / \partial V_i \partial V_j$  is a symmetric  $N \times N$   
 483 Hessian matrix, and  $\Delta V$  is the column vector given by

484 
$$\Delta V = \{\Delta u, \Delta w, \Delta p\}^T = \{u^{K+1} - u^K, w^{K+1} - w^K, p^{K+1} - p^K\}^T.$$

485 Given  $V^K$  from the previous iteration, (48) is a linear matrix equation that is solved at  
 486 each iteration for the  $N$  new variables  $V^{K+1}$ . In view of (46) and (47), the Hessian  
 487 matrix  $M(u, w)$  may be decomposed into several submatrices, as follows

488 
$$M(u, w) = \begin{bmatrix} M_{UU}(u, w) & M_{UW}(u, w) & M_{UP} \\ M_{UW}^T(u, w) & M_{WW}(u, w) & M_{WP} \\ M_{UP}^T & M_{WP}^T & 0 \end{bmatrix}. \quad (49)$$

489 Submatrices  $M_{UW}(u, w) = \partial^2 \mathcal{M} / \partial u \partial w$ , etc., depend nonlinearly on  $u, w$ . Thus,

490  $M_{UU}(u, w)$ ,  $M_{WW}(u, w)$  are square  $n_u \times n_u$ ,  $n_w \times n_w$  symmetric matrices, respectively,

491 while  $M_{UW}(u, w)$  is a rectangular  $n_u \times n_w$  matrix since  $n_u, n_w$  may not be equal. As noted

492 earlier,  $M_{WP}^T$  is an  $n_p \times n_w$  matrix and therefore not square unless  $n_p = n_w$ .

493

## 494 4.2 Blatter-Pattyn Discretizations

495

496 For completeness, we express the Blatter-Pattyn approximations from §3.4 in matrix  
 497 form, as follows

498 (1) The standard Blatter-Pattyn model from §3.4.1 takes the simple form

499 
$$R^{BP}(u) = \mathcal{M}_U(u, 0) + F_U = 0, \quad (50)$$

500 whose Newton-Raphson iteration is given by

501 
$$M^{BP}(u^K) \Delta u + R^{BP}(u^K) = 0, \quad (51)$$

502 and therefore the Blatter-Pattyn Hessian matrix is given by  $M^{BP}(u) = M_{UU}(u, 0)$ .

503 (2) The extended Blatter-Pattyn approximation from §3.4.2 becomes

$$504 \quad R^{EBP}(u, w, p) = \begin{bmatrix} \mathcal{M}_U(u, 0) + M_{UP}p + F_U \\ M_{WP}p \\ M_{UP}^T u + M_{WP}^T w \end{bmatrix} = 0, \quad (52)$$

505 with the Newton-Raphson iteration given by

$$506 \quad M^{EBP}(u^K) \Delta V + R^{EBP}(u^K, w^K, p^K) = 0, \quad (53)$$

507 and the associated Hessian matrix is

$$508 \quad M^{EBP}(u) = \begin{bmatrix} M_{UU}(u, 0) & 0 & M_{UP} \\ 0 & 0 & M_{WP} \\ M_{UP}^T & M_{WP}^T & 0 \end{bmatrix}. \quad (54)$$

509

## 510 **4.3 Solvability Issues**

### 511 **4.3.1 Solvability of Stokes and Blatter-Pattyn Models**

512

513 We now consider the solution of the three linear matrix problems (48), (51), (53)  
 514 associated with the Stokes and the corresponding Blatter-Pattyn approximate models.  
 515 While there are no issues in the continuous case, this is not so in the discrete case  
 516 depending on the choice of the grid and the finite elements, as noted earlier. The discrete  
 517 system to be solved has the general form

$$518 \quad \mathbf{M} \begin{Bmatrix} \mathbf{u} \\ p \end{Bmatrix} = \begin{bmatrix} A & B \\ B^T & 0 \end{bmatrix} \begin{Bmatrix} \mathbf{u} \\ p \end{Bmatrix} = \begin{Bmatrix} \mathbf{f} \\ g \end{Bmatrix}, \quad (55)$$

519 where  $\mathbf{u} = \{u, w\}^T$  in the linear case or  $\{\Delta u, \Delta w\}^T$  in the nonlinear case, and similarly for  
 520 the vector of pressures or pressure increments  $p$ . The form (55) is characteristic of  
 521 Stokes-type problems, or more generally of constrained minimization problems using  
 522 Lagrange multipliers. In finite element terminology these are called “mixed” or “saddle  
 523 point” problems, meaning that velocity components and the pressure occupy different  
 524 finite element spaces, and that the solution of (55) is actually at the saddle point with  
 525 respect to the velocity and pressure variables of the quadratic form associated with (55).  
 526 The matrix  $\mathbf{M}$  is symmetric but indefinite, with both positive and negative eigenvalues.  
 527 As a result, the matrix inverse may not be bounded and may lack stability.

528

529           There are three cases to consider:

530           (1) The standard Blatter-Pattyn model, (51). In this case only the matrix  $A$   
 531 exists, it is elliptic, and  $B = B^T = 0$ . As a result, the standard Blatter-Pattyn model is a  
 532 well-behaved and stable unconstrained minimization problem. The model (51) is self-  
 533 contained and is solved for  $u$  while the vertical velocity  $w$  is potentially available a  
 534 posteriori from a separately obtained continuity equation.

535           (2) The extended Blatter-Pattyn model, (53), (54). The middle row of the Hessian  
 536 (54) indicates that the solution for the pressure will be zero. Using this in the top row of  
 537 the Hessian, one obtains the standard Blatter-Pattyn system and therefore the same well-  
 538 behaved horizontal velocity  $u$  as above, with the result that the bottom row of the  
 539 Hessian, the continuity equation, is the only way to obtain a solution for the vertical  
 540 velocity  $w$ . However, this is possible only if matrix  $M_{WP}^T$  is invertible, which at  
 541 minimum requires a square matrix, i.e.,  $n_p = n_w$ , and this depends on the finite element  
 542 grid chosen for the discretization. For example, the popular second-order Taylor-Hood  
 543 (P2-P1) element with piecewise quadratic velocity and linear pressure (Hood and Taylor,  
 544 1973) typically has  $n_p \ll n_w$ . As a result, the linear system for  $w$  is greatly  
 545 underdetermined and cannot be solved for  $w$ . In fact, this is a problem for all inf-sup  
 546 stable elements with  $n_p \neq n_w$ , such as the Taylor-Hood element, for example.

547           (3) The standard and transformed Stokes models, (48), (49). These models  
 548 require the use of pressure as a Lagrange multiplier to enforce incompressibility and  
 549 therefore these are mixed or saddle point problems, as mentioned previously. To avoid  
 550 problems with the solution these finite elements must satisfy a certain condition, the  
 551 Ladyzhenskaya–Babuška–Brezzi (LBB, or inf-sup) condition. There is a very large  
 552 literature on the subject, e.g., Boffi et al. (2008), Elman et al. (2014), Auricchio et al.  
 553 (2017). Both the standard and transformed Stokes models are subject to this problem and  
 554 in general must use inf-sup stable finite elements. Testing for stability is not trivial.  
 555 However, collections of inf-sup stable elements for the Stokes equations may be found in  
 556 many papers and books on mixed methods, e.g., Boffi et al. (2008). The popular second-  
 557 order Taylor-Hood P2-P1 element (Hood and Taylor, 1973) is an example of an inf-sup  
 558 stable element. Some results involving this element are shown in Fig. 13 for Test B, one  
 559 of the test problems described in Appendix A.

560

### 561 4.3.2 A Special Case: Invertible Continuity Equation

562

563 In the continuous case, the Blatter-Pattyn approximation (§3.4.1) implies that vertical  
 564 velocity  $w$  is obtainable from the continuity equation after having solved for the  
 565 horizontal velocities  $u, v$ . As mentioned previously, this is possible to do in the  
 566 continuum but not necessarily so in the discrete case. The 2D discrete continuity  
 567 equation from (47) or (52) is given by

$$568 \quad M_{UP}^T u + M_{WP}^T w = 0. \quad (56)$$

569 For this to be solvable for  $w$  in terms of the horizontal velocity, i.e.,  $w(u)$ , means that

570 matrix  $M_{WP}^T$  must be invertible and thus it must be square and full rank. Since in general

571  $M_{WP}^T$  is an  $n_p \times n_w$  matrix, for solvability at minimum this requires that

$$572 \quad n_p = n_w. \quad (57)$$

573 Assuming that we are dealing with reasonable discretizations, we shall presume for our  
 574 discussion that matrix  $M_{WP}^T$  is always full rank. If Lagrange multipliers were to be used,  
 575 this means that the number of unknown pressures  $n_p$  would have to be augmented by the  
 576 number of Lagrange multipliers so (57) would become  $n_p + \lambda_z + \Lambda = n_w$  (See Appendix  
 577 B, §B2, for more details). We shall refer to (57) (together with the assumption of full  
 578 rank) as the solvability condition. In Appendix B we present several grids and elements  
 579 that satisfy this condition, including one variant in particular, the P1-E0 element, that will  
 580 be used in most of the 2D test problems featured in this paper. Thus, if the solvability  
 581 condition is satisfied, the discrete continuity equation (56) may be inverted for the  
 582 vertical velocity, to obtain

$$583 \quad w(u) = -M_{WP}^{-T} M_{UP}^T u, \quad (58)$$

584 where matrix  $M_{WP}^{-T}$  is defined by

$$585 \quad M_{WP}^{-T} = \left( M_{WP}^T \right)^{-1} = \left( M_{WP}^{-1} \right)^T. \quad (59)$$

586 Here we have used the fact that if matrix  $M_{WP}^T$  is invertible then so is its transpose  $M_{WP}$ .

587 Note that (58) is one discrete form of equation (43).

588

589 Invertibility of the continuity equation has several important applications. First, it  
 590 is a necessary requirement for the new Stokes approximations that are discussed in §6.2.

591 Since these approximations are based on approximating the vertical velocity in the  
 592 transformed second invariant, (28), it is necessary to obtain the vertical velocity  
 593 independently of solving the entire coupled Stokes problem. Second, we noticed earlier  
 594 that the extended Blatter-Pattyn model does not work with a Taylor-Hood P2-P1 grid  
 595 because the solvability condition is not satisfied. However, this model does work with a  
 596 variant of the Taylor-Hood grid, the P2-E1 grid, illustrated in Fig. 13A, which does  
 597 satisfy the solvability condition and this therefore allows for a successful calculation of  
 598 the vertical velocity.

599

600 Perhaps the main reason for the importance of the solvability condition is that it  
 601 implies that the Stokes variational principle, (15) or (33), may be transformed into and  
 602 therefore that it is equivalent to an optimization or minimization problem. Consider the  
 603 discrete form of the variational functional given by (46). Working with a grid that  
 604 satisfies the solvability condition, we may substitute the vertical velocity given by (58)  
 605 into the functional (46). This immediately eliminates the term responsible for the  
 606 continuity equation, including the pressure, and one obtains a functional in terms of  
 607 horizontal velocity  $u$  only, as follows

$$608 \quad \mathcal{A}(u) = \mathcal{M}(u, w(u)) + u^T F_U + w(u)^T F_W. \quad (60)$$

609 Since the functional  $\mathcal{M}(u, w(u))$  is positive semi-definite, this is now an unconstrained  
 610 minimization problem, entirely analogous to the standard Blatter-Pattyn problem of  
 611 §3.4.1 except that here it represents the full Stokes problem for either the standard ( $F_W$ )  
 612 or the transformed ( $F_U$ ) formulation. This result suggests that a conventional Stokes  
 613 problem, when solved on a grid satisfying the solvability condition, is equivalent to an  
 614 unconstrained minimization problem and therefore is well behaved. This is because any  
 615 problem will give the same answer whether formulated as (46) or (60) on a grid that  
 616 satisfies the solvability condition.

617

618 Note that functional (60) is actually the discrete version of a pressure-free  
 619 formulation that was attempted analytically by Dukowicz (2012). It is possible to  
 620 consider solving problems in practice using the pressure-free formulation (60) instead of  
 621 a standard saddle point formulation such as (46) or (47). However, this produces a dense  
 622 Hessian matrix that makes a solution using Newton-Raphson iteration very costly and  
 623 therefore impractical, particularly for large problems.

624



## 5. Comparison of the Standard and Transformed Stokes Models

The standard and transformed Stokes models are expected to converge to the same solution. To verify that this is indeed the case we do a number of calculations for some 2D test problems based on the ISMIP-HOM benchmark (Pattyn et al, 2008). These tests are described in Appendix A where they are referred to as Test B and Test D\*. Test B involves no-slip boundary conditions on a sinusoidal bed, and Test D\* evaluates sliding of the ice sheet along a flat bed in the presence of sinusoidal friction. The tests are discretized using P1-E0 elements on a regular grid composed of  $n$  quadrilaterals in the  $x$ -direction and  $m$  quadrilaterals in the  $z$ -direction, illustrated in Fig. B1, with each quadrilateral divided into two triangles. Results are presented for two domain lengths,  $L = 5$  km and 10 km, to test the aspect ratio range where the Blatter-Pattyn model begins to fail, and using a relatively coarse grid, i.e.,  $m = n = 40$ , except when we consider the convergence of the models with grid refinement in Fig. 3.

Fig. 3 evaluates the convergence of the two Stokes models as a function of grid resolution  $r$ , where  $r$  is the number of quadrilaterals in either direction. The models do converge to the same solution and convergence is second order as expected from the use of linear elements. Interestingly, the transformed Stokes model displays considerably smaller error at all resolutions in Test B. As a result, we observe that standard Stokes calculations are not fully converged even at the 40x40 resolution.

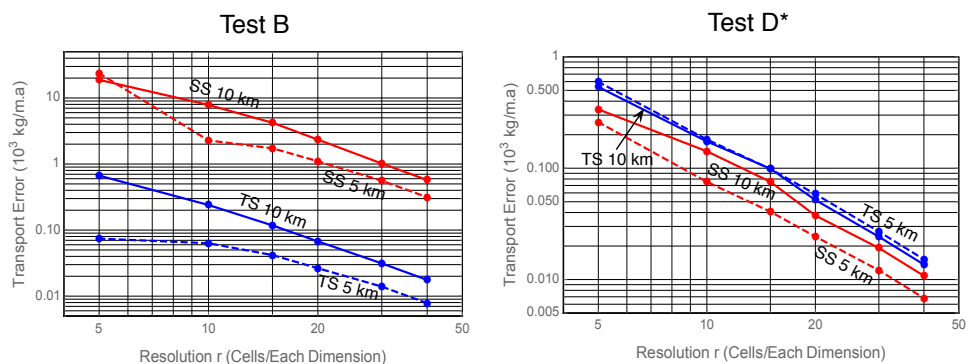
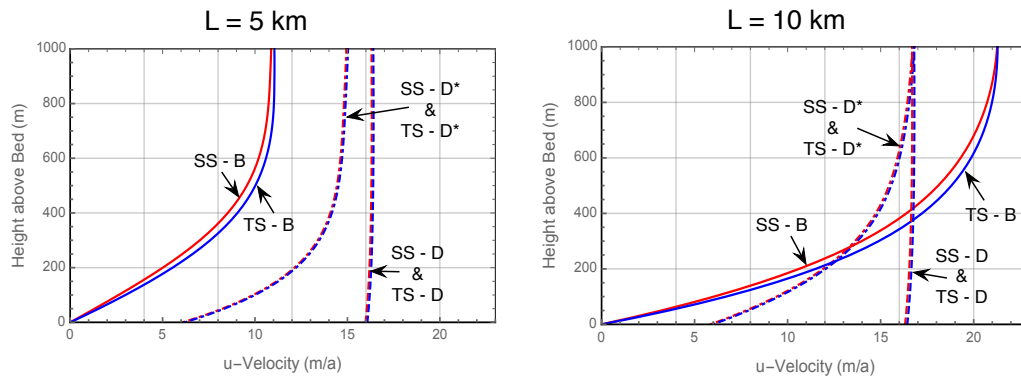


**Figure 3.** Convergence of ice transport in Tests B and D\* with grid refinement. Transformed Stokes (TS) plots are in blue and standard Stokes plots (SS) are in red.

Fig. 4 shows the vertical profiles of the horizontal velocity  $u$  at outflow,  $x = L$ . We plot results from the no-slip Test B problem and the two frictional sliding problems, Tests D and D\*. The Test D profile from the ISMIP-HOM benchmark is almost

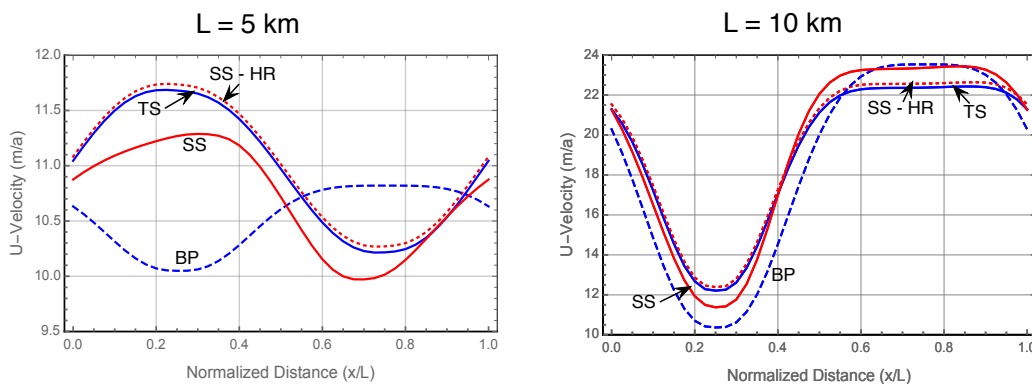
653 vertically constant, indicating that the value for basal friction originally chosen is too  
 654 small. This is what motivated the change from Test D to Test D\* in Appendix A.



655 **Figure 4.** The  $u$ -velocity profile at location  $x = L$  as a function of height from the bed.  
 656  
 657

658 Figs. 5 and 6 show the  $u$ -velocity at the ice sheet upper surface for Tests B and  
 659 D\*. This is the benchmark used in ISMIP-HOM to compare the different ice sheet  
 660 models. Here we compare four cases: the standard Stokes model (SS), the transformed  
 661 Stokes model (TS), the Blatter-Pattyn (BP) model, and for reference, a very high  
 662 resolution full-Stokes Test B calculation “oga1” (SS-HR), available from the ISMIP-  
 663 HOM paper and also independently available in Gagliardini and Zwinger (2008). The TS  
 664 and the SS-HR plots lie on top of one another (they have been offset slightly for clarity),  
 665 indicating that the TS model is already fully converged. We again observe that the SS  
 666 model is not yet converged in Test B, particularly at  $L = 5$  km. As also seen in the  
 667 ISMIP-HOM paper, the Blatter-Pattyn calculation (BP) shows large deviations from the  
 668 Stokes results, especially so at  $L = 5$  km where the surface velocity is entirely out of  
 669 phase with the Stokes results. Test D\* results in Fig. 6 for the SS and TS models are very  
 670 similar (the SS plot has been slightly offset upward for visibility). As expected, the error  
 671 in the Blatter-Pattyn results is noticeable at  $L = 10$  km and very large at  $L = 5$  km.  
 672

673 Pressure results are not shown because, particularly in the transformed case,  
 674 pressure has little or no physical significance. However, pressures calculated on the P1-  
 675 E0 grid are particularly smooth and well behaved.

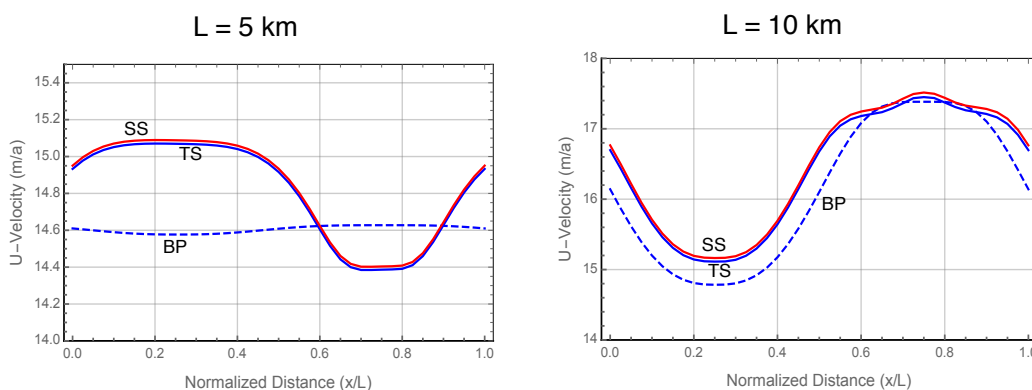


676

677

**Figure 5.** Upper surface u-velocity,  $u(x, z_s)$  - Test B, No-slip boundary conditions.

678



679

680

**Figure 6.** Upper surface u-velocity,  $u(x, z_s)$  - Test D\*, Modified frictional sliding case.

681

## 6. Applications of the Transformed Stokes Model

### 6.1 Adaptive Switching between Stokes and Blatter-Pattyn Models

684

685 One way of reducing the cost of a full Stokes calculation is to use it adaptively with a  
 686 cheaper approximate model. That is, one may use the cheaper model in those parts of a  
 687 problem where it is accurate, and the more expensive full Stokes model where the  
 688 approximate model loses accuracy. One example of such an adaptive approach is the  
 689 tiling method by Seroussi et al. (2012). However, there are drawbacks to such methods,  
 690 such as the difficulty of incorporating two or more presumably quite different models  
 691 into a single model, and the additional complexity of a necessary transition zone to  
 692 couple the disparate models.

693

694

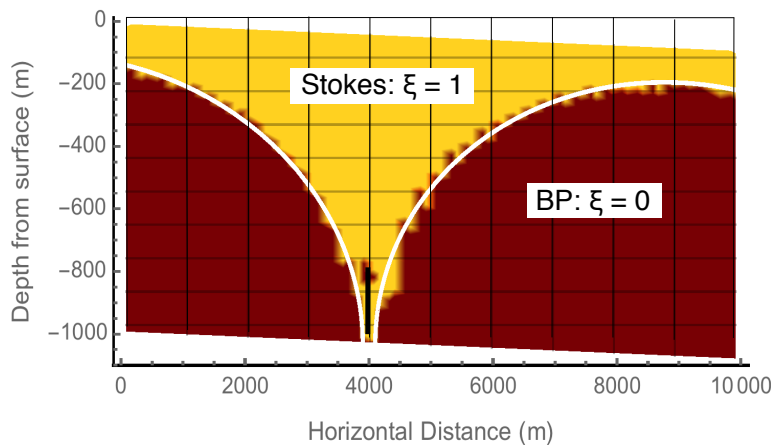
695

The transformed Stokes model used in such an adaptive role is attractive because it may be switched between the Stokes and Blatter-Pattyn cases simply by switching the

696 parameter  $\xi \in \{0,1\}$  between its two values. For simplicity the extended Blatter-Pattyn  
 697 approximation ( $\xi = 0, \hat{\xi} = 1$ ) is being used since both the Stokes and the Blatter-Pattyn  
 698 parts of the code have the same number of discrete variables. The extended Blatter-  
 699 Pattyn model requires the use of a grid that satisfies the solvability condition as explained  
 700 in §4.3. We therefore use the P1-E0 element. However, it would be computationally  
 701 cheaper to use the standard Blatter-Pattyn approximation ( $\xi, \hat{\xi} = 0$ ) instead, solving only  
 702 for the horizontal variables and coupling to the Stokes model with  $p = 0$  and  $w = w(u, v)$   
 703 at the interface. This, however, implies much more complicated programming.

704

705 To demonstrate the idea of adaptive switching with a transformed Stokes model,  
 706 we introduce a new test problem, Test O, described in Appendix A and illustrated in Fig.  
 707 A1. This consists of an inclined ice slab whose movement is obstructed by a thin  
 708 obstacle protruding 20% of the ice depth up from the bed. No-slip boundary conditions  
 709 are applied along the bed and on the obstacle itself. Because of the localized nature of  
 710 the obstacle, the Blatter-Pattyn approximation conditions, (38), must fail near the obstacle  
 711 and therefore the full Stokes model is needed for good accuracy, at least locally.



712

713 **Figure 7.** Mask function (white curve,  $z = F_M(x)$ ) to indicate where the Stokes and BP  
 714 models are activated in the 20% obstacle test problem. The dark brown region delineates  
 715 the region where  $|\partial w / \partial x| \leq 0.1 |\partial u / \partial z|$  in a Blatter-Pattyn calculation.

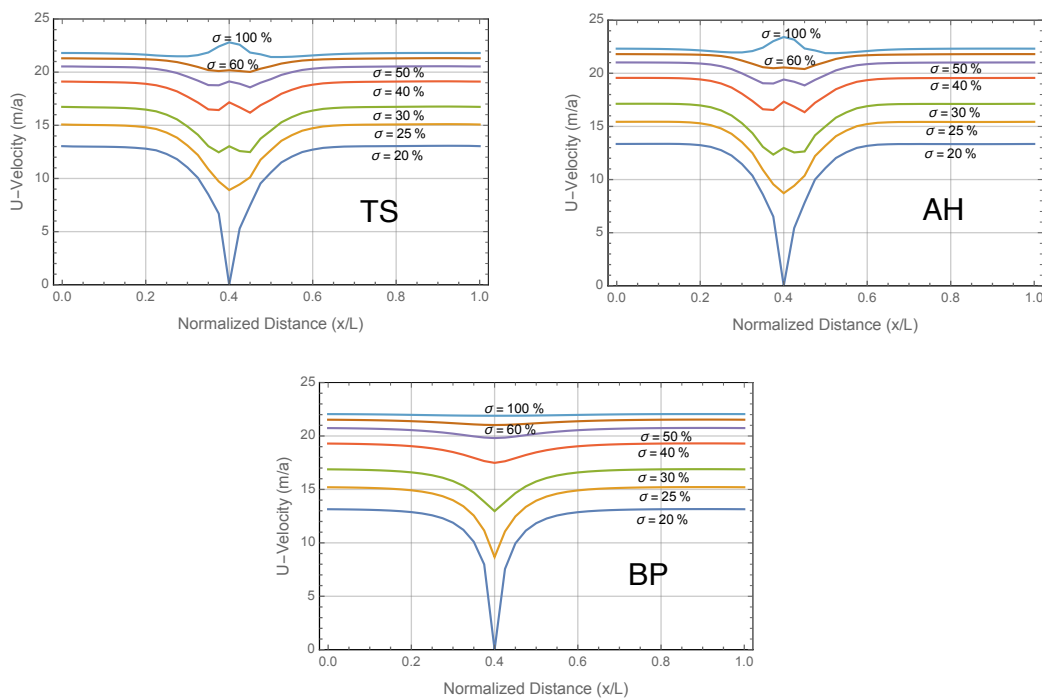
716

717 To implement this, we first use a Blatter-Pattyn calculation to outline regions  
 718 where  $|\partial w / \partial x| \leq 0.1 |\partial u / \partial z|$ , approximately localizing where the Blatter-Pattyn

719 approximation is valid. This determines a mask function  $z = F_M(x)$ , illustrated in Fig. 7  
 720 by the white curves, that specifies where the two models must be used. Defining the  
 721 centroid of a triangular element by  $(x_C, z_C)$ , the code makes a selection in each element:

$$722 \quad \begin{aligned} z_C \leq F_M(x_C) &\Rightarrow \text{Set } \xi = 0, \text{ i.e., the Blatter-Pattyn region,} \\ z_C > F_M(x_C) &\Rightarrow \text{Set } \xi = 1, \text{ i.e., the Stokes region.} \end{aligned}$$

723 Somewhat counterintuitively, the Stokes region occupies the upper part of the domain in  
 724 Fig. 7 and includes the obstacle, while the Blatter-Pattyn region occupies much of the  
 725 bottom part of the domain. A transition zone, e.g.,  $0 \leq \xi(x, z) \leq 1$ , is possible but was not  
 726 used in the present calculation.



727  
 728 **Figure 8.** Comparing results for the Transformed Stokes (TS),  
 729 the Adaptive-Hybrid (AH), and the Blatter-Pattyn (BP) models in Test O.

730  
 731 The Adaptive-Hybrid results are shown in Fig. 8, which shows curves of the  
 732 horizontal velocity  $u$  at seven different vertical positions specified as a percentage of the  
 733 distance between top and bottom, with  $\sigma = 100\%$  at the top surface. The top right panel  
 734 shows the results for the adaptive-hybrid model (AH). For comparison, the top left panel  
 735 and the bottom panel show results for the Stokes (TS) and the Blatter-Pattyn (BP)  
 736 calculations, respectively. All calculations are at the 40x40 resolution. The Adaptive-  
 737 Hybrid results are very similar to the full Stokes results, reproducing most features of the

738 velocity profiles, including the velocity bump at the top surface, indicating that even the  
 739 top surface feels the presence of the obstacle. The Blatter-Pattyn results are much less  
 740 accurate; they completely miss the details of the flow near the obstacle. We also measure  
 741 the RMS error in the  $u$ -velocity relative to the Stokes results. The RMS error in the  
 742 Blatter-Pattyn case is 0.493 m/a and 0.440 m/a in the Adaptive-Hybrid case, smaller in  
 743 the Blatter-Pattyn case as expected, but the difference is not as large and striking as the  
 744 visual difference in Fig. 8. Nevertheless, the adaptive-hybrid method is successful  
 745 judged by the Fig. 8 results alone. Unfortunately, an estimate of the computational cost  
 746 savings will have to wait a more realistic implementation.

747

## 748 **6.2. Two Stokes Approximations Beyond Blatter-Pattyn**

749

750 As shown in §3.4, simply setting  $w = 0$  in the second invariant  $\tilde{\epsilon}^2$  in the transformed  
 751 functional  $\tilde{\mathcal{A}}$  **results in the standard Blatter-Pattyn approximation**. This suggests that  
 752 approximating the vertical velocity  $w$  in the functional would be a good way to create  
 753 approximations that improve on the Blatter-Pattyn approximation since  $w = 0$  already  
 754 produces an excellent approximation. We will look at two such methods in this Section  
 755 although others are possible. The first method, to be called the BP+ approximation, is  
 756 implemented using a combination of Newton and Picard iterations such that at each  
 757 Newton iteration the pressure-free variational functional is evaluated using a lagged  
 758 vertical velocity  $w^K$  from the previous iteration. The pressure is used in a subordinate  
 759 role as a “test function” to obtain a decoupled invertible continuity equation to obtain  
 760  $w(u^K)$ . Although this method improves on the accuracy of the Blatter-Pattyn  
 761 approximation, its overall accuracy is limited because it uses only the horizontal  
 762 momentum equation and neglects the vertical momentum equation. The second method,  
 763 to be called the Dual-Grid approximation, keeps the pressure and vertical velocity as in  
 764 the transformed Stokes model but approximates it by discretizing the continuity equation  
 765 on a coarser grid. Since vertical velocity  $w$  is determined by inverting the continuity  
 766 equation, this has the effect of approximating the vertical velocity while reducing the  
 767 number of pressure and vertical velocity variables. This preserves the structure of the  
 768 Stokes model, while the degree of approximation is determined by the amount of  
 769 coarsening of the continuity grid.

770

771 **6.2.1 An Improved Blatter-Pattyn or BP+ Approximation**

772

773 To prepare, we introduce a pair of 2D variational quasi-functionals,  $\tilde{\mathcal{A}}_{PS1}[u]$  and  
 774  $\tilde{\mathcal{A}}_{PS2}[\tilde{P}]$ . Noting that  $\tilde{P} = 0$  in the Blatter-Pattyn approximation, we drop the pressure  
 775 term from the transformed functional (33) and define a new pressure-free functional,

$$776 \quad \tilde{\mathcal{A}}_{PS1}[u] = \int_V dV \left[ \frac{4n}{n+1} \eta_0 (\tilde{\epsilon}^2)^{(1+n)/2n} + \rho g u \frac{\partial z_s}{\partial x} \right] \quad (61)$$

$$+ \frac{1}{2} \int_{S_{B2}} dS \beta(x) \left( u^2 + \zeta \left( u n_x / n_z \right)^2 \right),$$

777 where

$$778 \quad \tilde{\epsilon}^2 = \left( \frac{\partial u}{\partial x} \right)^2 + \frac{1}{4} \left( \frac{\partial u}{\partial z} + \frac{\partial w}{\partial x} \right)^2. \quad (62)$$

779 Since the continuity equation has been eliminated from (61), incompressibility is  
 780 introduced separately by defining a second functional,

$$781 \quad \tilde{\mathcal{A}}_{PS2}[p] = \int_V dV p \left( \frac{\partial u}{\partial x} + \frac{\partial w}{\partial z} \right). \quad (63)$$

782 Note that functional (61) is a function of  $u, w$  but variation is to be taken only with  
 783 respect to  $u$ , and similarly, functional (63) is a function of  $u, w, p$  but variation is taken  
 784 only with respect to  $p$ . Direct substitution is used for boundary conditions, as before.  
 785 Here we are effectively viewing the pressure  $p$  as a “test function” in the finite element  
 786 sense. This gives us great flexibility to create elements that satisfy the solvability  
 787 condition (57) as desired. In a triangulation, for example, pressures may be assigned to  
 788 every two triangles, as in a P1-E0 grid, while others may be assigned to a single triangle  
 789 so as to achieve an equal number of pressure and vertical velocity variables.

790

791 The variation of  $\tilde{\mathcal{A}}_{PS1}[u]$  with respect to  $u$ , results in a set of  $n_u$  discrete Euler-  
 792 Lagrange equations,

$$793 \quad \hat{R}_U(u, w) = \frac{\partial \tilde{\mathcal{A}}_{PS1}(u, w)}{\partial u} = M_U(u, w) + F_U = 0. \quad (64)$$

794 This may be recognized as the Blatter-Pattyn model, (50), when  $w$  is set to zero. The  
 795 discrete variation of  $\tilde{\mathcal{A}}_{PS2}[p]$  with respect to  $p$ , results in the continuity equation, (56),

796 
$$\hat{R}_p(u, w) = \frac{\partial \tilde{\mathcal{A}}_{PS2}(u, w, p)}{\partial p} = M_{UP}^T u + M_{WP}^T w = 0. \quad (65)$$

797 These two systems are now combined to form the BP+ approximation, as follows

798 
$$\hat{R}(u, w) = [\hat{R}_U(u, w), \hat{R}_P(u, w)]^T = 0. \quad (66)$$

799 This is a single system of  $n_u + n_p$  equations to determine the  $n_u + n_w$  discrete variables  
800  $u, w$ , implying that (66) is viable only on grids satisfying the solvability condition,  
801  $n_p = n_w$ . Just as in the standard Blatter-Pattyn approximation in §3.4.1, the vertical  
802 momentum equation is missing, but instead of neglecting  $w$ , the vertical velocity is now  
803 consistently obtained from the continuity equation.

804

805 The continuum version of the discrete Euler-Lagrange system (64), (65) may be  
806 written as follows

807 
$$\frac{\partial}{\partial x} \left( 4\tilde{\mu} \frac{\partial u}{\partial x} \right) + \frac{\partial}{\partial z} \left( \tilde{\mu} \left( \frac{\partial u}{\partial z} + \frac{\partial w}{\partial x} \right) \right) - \rho g \frac{\partial z_s}{\partial x} = 0, \quad (67)$$

$$\frac{\partial u}{\partial x} + \frac{\partial w}{\partial z} = 0,$$

808 whose the boundary conditions are

809 
$$\left. \begin{aligned} 4\tilde{\mu} \frac{\partial u}{\partial x} n_x + \tilde{\mu} \left( \frac{\partial u}{\partial z} + \frac{\partial w}{\partial x} \right) n_z &= 0 \text{ on } S_S, \quad u = w = 0 \text{ on } S_{B1}, \\ 4\tilde{\mu} \frac{\partial u}{\partial x} n_x + \tilde{\mu} \left( \frac{\partial u}{\partial z} + \frac{\partial w}{\partial x} \right) n_z + \beta(x) \left( u + \zeta u (n_x/n_z)^2 \right) &= 0, \\ w &= -u n_x / n_z, \end{aligned} \right\} \text{ on } S_{B2}, \quad (68)$$

810 where  $\tilde{\mu} = \eta_0 \left( \tilde{\epsilon}^2 \right)^{(1-n)/2n}$  and the second invariant  $\tilde{\epsilon}^2$  is given by (62). Remarkably, a  
811 model exactly equivalent to (67), i.e., the BP+ approximation, was introduced by  
812 Hererich (1987) to study the transition zone between an ice sheet and an ice shelf<sup>1</sup>. This  
813 predates the less accurate, widely used Blatter-Pattyn model by some eight years.  
814 Unfortunately, this anticipatory work seems to have faded into obscurity.

815

816 There are two ways of solving the BP+ system (66), as follows

---

<sup>1</sup> Reference pointed out to me by C. Schoof.



817 (1) BP+, Quasi-variational, Newton iteration version:

818 Although a single variational principle does not exist in this case, it is still  
 819 possible to make use of Newton-Raphson iteration to obtain second order convergence.  
 820 To do this, we treat (66) as a single multidimensional nonlinear system and solve it using  
 821 Newton-Raphson iteration, as follows

$$822 \quad \begin{bmatrix} M_{UU}(u^K, w^K) & M_{UW}(u^K, w^K) \\ M_{UP}^T & M_{WP}^T \end{bmatrix} \begin{bmatrix} \Delta u \\ \Delta w \end{bmatrix} + \begin{bmatrix} \hat{R}_U(u^K, w^K) \\ \hat{R}_P(u^K, w^K) \end{bmatrix} = 0, \quad (69)$$

823 where  $M_{UU}(u, w) = \partial \hat{R}_U(u, w) / \partial u$  and  $M_{UW}(u, w) = \partial \hat{R}_U(u, w) / \partial w$  are the same  
 824 matrices as appear in (49). Convergence is rapid (quadratic) once in the basin of  
 825 attraction but each step is more expensive than the Picard iteration described next.

826

827 (2) BP+, Newton/Picard iteration version:

828 A single step of the Newton-Raphson system (69) may be written as follows

$$829 \quad \begin{aligned} M_{UU}(u^K, w^K) \Delta u + M_{UW}(u^K, w^K) \Delta w + \hat{R}_U(u^K, w^K) &= 0, \\ M_{UP}^T u^{K+1} + M_{WP}^T w^{K+1} &= 0. \end{aligned} \quad (70)$$

830 If we lag the vertical velocity, i.e.,  $w^{K+1} = w^K \Rightarrow \Delta w = 0$  in the first equation, we obtain a  
 831 Picard iteration algorithm as follows

Starting from  $K = 0$ , choose an initial guess,  $u^0 \neq 0, w(u^0)$ ,

Solve:

$$832 \quad \begin{aligned} M_{UU}(u^K, w^K) \Delta u + \hat{R}_U(u^K, w^K) &= 0, \\ u^{K+1} &= u^K + \Delta u, \\ w^{K+1} &= w(u^{K+1}) = -M_{WP}^{-T} M_{UP}^T u^{K+1}, \\ K &= K + 1, \end{aligned} \quad (71)$$

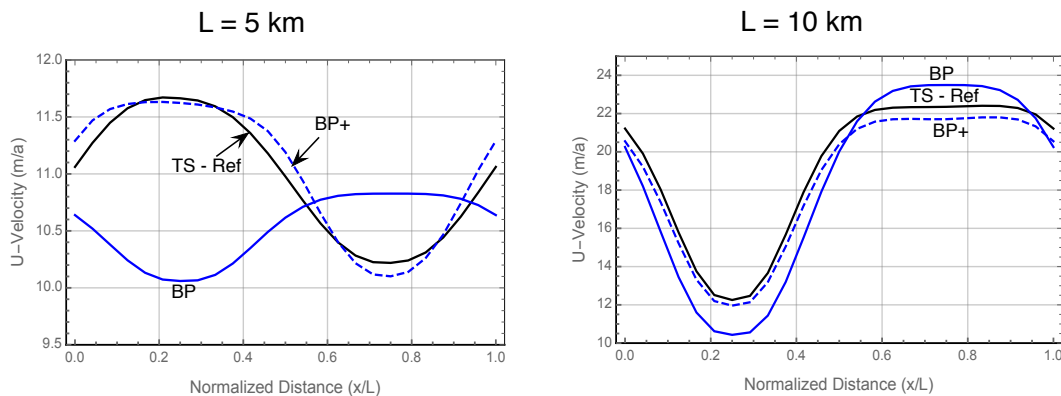
Repeat until convergence.

833 Each step of this iteration is inexpensive since it is equivalent to a step of the standard  
 834 Blatter-Pattyn model, (36). On the other hand, Picard iterations typically converge only  
 835 linearly. It remains to be seen which version is preferable in practice.

836

837 Both BP+ versions converge to the same solution. Fig. 9 compares the upper  
 838 surface u-velocity from the improved Blatter-Pattyn (BP+) approximation to the standard  
 839 Blatter-Pattyn approximation and to a reference exact Stokes calculation. The RMS u-  
 840 Error of the BP+ approximation relative to the exact Stokes case is shown in Fig. 12. The

841 BP+ approximation is noticeably more accurate than the BP approximation, particularly  
 842 in the  $L = 5$  km case where the Blatter-Pattyn solution bears no resemblance to the  
 843 correct solution while the BP+ approximation shows excellent accuracy. This is  
 844 confirmed by the RMS u-Error results in Fig. 12 where BP+ is two to three times as  
 845 accurate as BP.



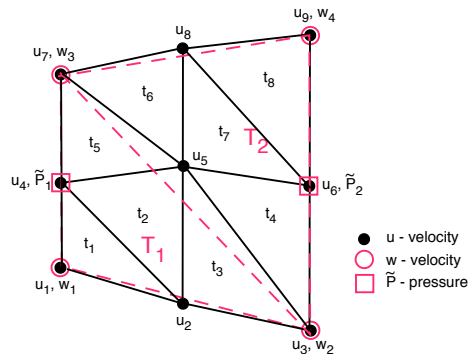
846  
 847 **Figure 9.** Comparing Approximations. Test B, Upper surface u-velocity.  
 848 TS-Ref: Transformed Stokes; BP: Blatter-Pattyn; BP+: Improved Blatter-Pattyn.  
 849 Resolution: 24x24.  
 850

851 These two versions depend on an invertible continuity equation to obtain  
 852  $w = w(u)$ . However, vertical velocity  $w$  may already be available for the purpose of  
 853 temperature advection in production code packages that either incorporate or are based on  
 854 the Blatter-Pattyn approximation. Thus, the BP+ approximation, and particularly the  
 855 Newton/Picard version, may be attractive for use in such codes since they improve the  
 856 accuracy of the basic Blatter-Pattyn model, as seen in Fig. 9, at little additional cost.  
 857

### 858 6.2.2 A “Dual-Grid” Transformed Stokes Approximation

859  
 860 Here we take a different approach and approximate the continuity equation in the  
 861 transformed Stokes model, which indirectly approximates  $w$ . Thus, the continuity  
 862 equation is discretized on a grid coarser than the one used for the momentum equations,  
 863 and then interpolate the vertical velocity to appropriate locations on the finer grid. This  
 864 reduces the number of unknown variables in the problem, making it cheaper to solve but  
 865 hopefully without much loss of accuracy. As described in Appendix A, our test problem  
 866 grids are logically rectangular, divided into  $n$  cells horizontally and  $m$  cells vertically.  
 867 The coarse grid is constructed by dividing the fine grid into  $s$  equal segments in each  
 868 direction. This assumes that the integers  $n$  and  $m$  are each divisible by  $s$ , such that

869 there are  $nm/s^2$  coarse cells in total, with each coarse cell containing  $s^2$  fine cells. The  
 870 primary grid (i.e., the fine grid) was chosen to have  $n = m = 24$ , resulting in a reference  
 871  $24 \times 24$  fine grid, so as to maximize the number of different coarse grids that may be  
 872 used for this test. Coarse grids were constructed using  $s = 2, 3, 4, 6$ , and this resulted in  
 873 fine/coarse grid combinations labeled by  $24 \times 12, 24 \times 8, 24 \times 6, 24 \times 4$ , respectively.  
 874 Similar to a P1-E0 fine grid, coarse grid vertical velocities  $w$  are located at vertices and  
 875 pressures at vertical edges. Fig. 10 illustrates the case of a single coarse and four fine  
 876 quadrilateral cells for a grid fragment with  $n = m = 2$  and  $s = 1$ . For the Test B problem,  
 877 using direct substitution for basal boundary conditions, there will be  $nm$  u-variables and  
 878  $nm/s^2$  w- and p-variables each, for a total of  $nm(1 + 2/s^2)$  unknown variables,  
 879 considerably fewer than the  $3nm$  variables in the full resolution (i.e., fine grid) case,  
 880 depending on the value of  $s$ . The coarse grid terms in the functional that are affected,  
 881  $\tilde{P}(\partial u/\partial x + \partial w/\partial z)$  and  $\partial w/\partial x$ , are computed using coarse grid variables and  
 882 interpolated to the fine grid. We will consider two versions depending on how the coarse  
 883 grid terms are calculated and distributed on the fine grid.



884  
885

886 **Figure 10.** A Sample of a Coarse/Fine P1-E0 Grid for the Dual-Grid Approximation.

887 Resolution:  $n = m = 2, s = 1$ . Coarse grid is in red, fine grid in black.

888

889 (1) Approximation A, Bilinear interpolation:

890

Referring to Fig. 10, the four velocities at the vertices of the coarse grid

891

quadrilateral, i.e.,  $u_1, u_3, u_7, u_9$  and  $w_1, w_2, w_3, w_4$ , are used to obtain  $u, w$  at the remaining

892

five vertices of the fine grid by means of bilinear interpolation. Thus, the five velocities

893

$u_2, u_4, u_5, u_6, u_8$  are obtained in terms of vertex velocities  $u_1, u_3, u_7, u_9$ , and similarly for the

894

$w$  velocities. The resulting complete set of fine grid variables, interpolated from coarse

895 grid variables, are used calculate the divergence  $D = (\partial u / \partial x + \partial w / \partial z)$  and the quantity  
 896  $\partial w / \partial x$  in each of the eight triangular elements  $t_1, t_2, \dots, t_8$  of the fine grid. Coarse grid  
 897 pressures  $\tilde{P}_1, \tilde{P}_2$  are associated with the coarse grid triangles  $T_1, T_2$ . The products  $\tilde{P}_1 D$  in  
 898 elements  $t_1, t_2, t_3, t_5$  and  $\tilde{P}_2 D$  in elements  $t_4, t_6, t_7, t_8$  are then accumulated over the entire  
 899 grid to obtain  $\tilde{P}(\partial u / \partial x + \partial w / \partial z)$  for use in the transformed functional  $\tilde{\mathcal{A}}$ . Similarly, the  
 900 quantity  $\partial w / \partial x$  is computed in the fine grid elements from coarse grid variables for use  
 901 in the second invariant  $\tilde{\mathcal{E}}^2$ .

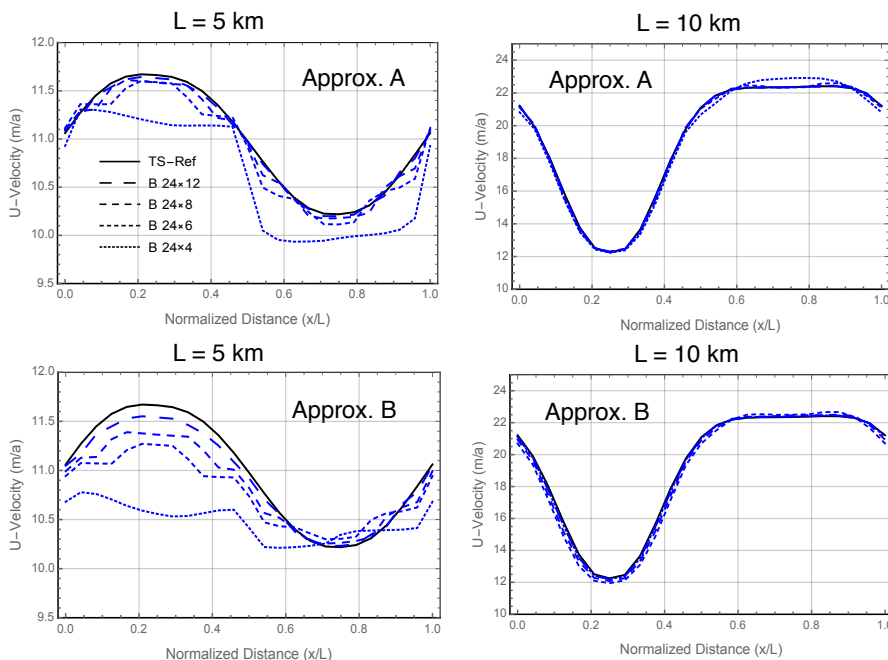
902

### 903 (2) Approximation B, Linear interpolation:

904 In this version, the three velocities at the vertices of the two coarse grid triangles  
 905  $T_1$  and  $T_2$ , i.e.,  $u_1, u_3, u_7$  and  $w_1, w_2, w_3$  in  $T_1$ , and  $u_7, u_3, u_9$  and  $w_3, w_2, w_4$  in  $T_2$ ,  
 906 approximate the divergence  $D = (\partial u / \partial x + \partial w / \partial z)$  and the quantity  $\partial w / \partial x$  as constant  
 907 values in the two coarse triangles. The constant quantities  $\tilde{P}_1 D$ ,  $\tilde{P}_2 D$  are then  
 908 accumulated over the entire grid. The constant quantity  $\partial w / \partial x$  in each coarse triangle is  
 909 then distributed to each of the eight fine grid elements  $t_1, t_2, \dots, t_8$  depending on whether  
 910 the centroid of the fine triangular element is in  $T_1$  or  $T_2$ . As in the previous case, this is  
 911 then used in the second invariant  $\tilde{\mathcal{E}}^2$  when evaluating the transformed functional  $\tilde{\mathcal{A}}$ .

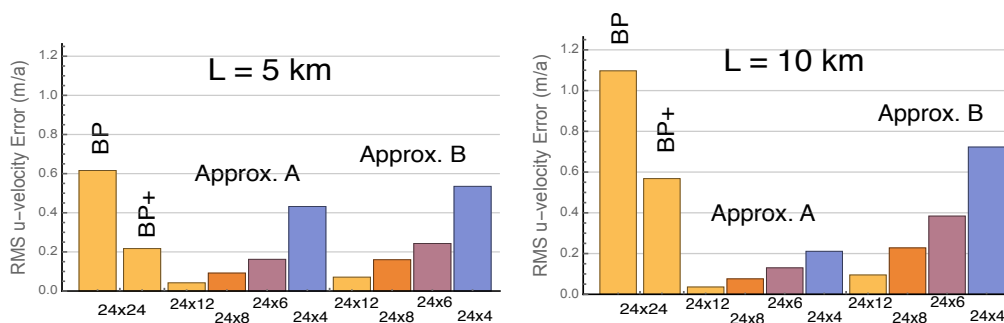
912

913 While the number and type of unknown variables is the same in the two versions,  
 914 they differ considerably in accuracy, as is seen in Figs. 11 and 12. Fig. 11 compares the  
 915 upper surface u-velocity in both version, Approximations A and B, for the four coarse  
 916 grid combinations and the reference 24x24 fine grid calculation. Fig. 12 compares the  
 917 overall accuracy the same way by means of the RMS u-Error. As might be expected, the  
 918 accuracy of Approx. A is better than the accuracy of Approx. B, particularly in the case  
 919 when  $L = 10$  km. Both versions are more accurate than the Blatter-Pattyn and BP+  
 920 approximations, except at the lowest 24x4 resolution when only the Approx. A version  
 921 retains that distinction.



922  
 923 **Figure 11.** Comparing Approximations A and B. Test B. Upper surface u-velocity.  
 924 TS-Ref: Reference Stokes 24x24; Fine/Coarse resolutions (r x R): 24xR, R=12, 8, 6, 4.  
 925

926 In summary, the dual-grid approximation improves on the Blatter-Pattyn  
 927 approximation in both versions and at all resolutions, as seen in Fig. 12. Compared to the  
 928 BP+ approximations, here the vertical momentum equation is retained, although in  
 929 approximated form. In fact, here the solution procedure is very similar to that of the  
 930 unapproximated Stokes model except that the dimensions of the pressure and the vertical  
 931 velocity variables are reduced.



932  
 933 **Figure 12.** Comparing RMS u-Error in Different Approximations, Test B,  
 934 Resolutions (r x R): Approx. BP, BP+: 24x24; Approx. A, B: 24xR, R=12, 8, 6, 4.  
 935

## 936 7. Second-Order Discretizations

937

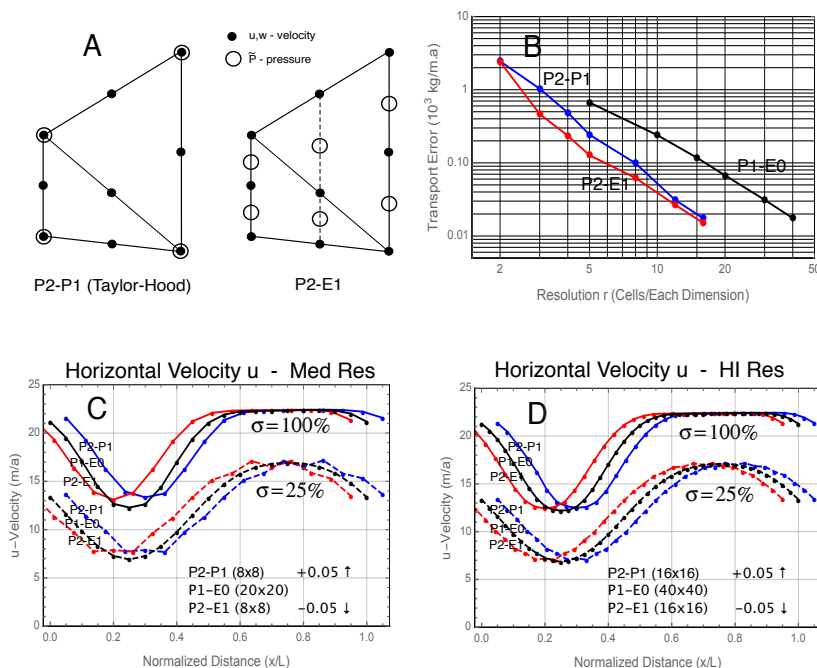
938 So far we have been using first-order elements, primarily P1-E0. However, in current  
 939 practice Stokes models are more often based on second-order elements such as the  
 940 popular Taylor-Hood P2-P1 element (Leng et al., 2012; Gagliardini et al., 2013). In 2D  
 941 the P2-P1 element, illustrated in Fig. 13A, has velocities on element vertices and edge  
 942 midpoints and pressures on element vertices, resulting in a quadratic velocity and linear  
 943 pressure distributions. The element satisfies the conventional inf-sup stability condition  
 944 (e.g., Elman et al., 2014) but not the solvability condition (57). For example, in Test B  
 945 with direct substitution for basal boundary conditions, the number of vertical velocity  
 946 variables is  $n_w = 4nm$ , much larger than the number of pressure variables,  $n_p = n(m+1)$ .

947

948 Stokes models work well with a Taylor-Hood grid, as illustrated in Fig. 13, where  
 949 both P2-P1 and P1-E0 models converge to a common Test B solution, but models that  
 950 require the solvability condition (57) will not work on a P2-P1 grid, as is the case with  
 951 the extended Blatter-Pattyn approximation. However, a second-order element can be  
 952 constructed that is consistent with an invertible continuity equation. This is called the  
 953 P2-E1 element and it is illustrated in Fig. 13A. It is second-order for velocities and linear  
 954 for pressure, just like the P2-P1 element, but the pressure is edge-based, as in the P1-E0  
 955 element. Pressure is located midway between the velocities on the vertical cell edges,  
 956 including an “imaginary” vertical edge joining the velocities in the middle of the vertical  
 957 column. Since pressures are collinear with vertical velocities along vertical grid edges, as  
 958 in the P1-E0 element, the same analysis in Appendix B demonstrates that this element  
 959 also satisfies the solvability condition (57). As explained in Appendix B, this grid should  
 960 be constructed using vertical columns of quadrilaterals. A 3D analog exists as explained  
 961 in Appendix B.

962

963 Fig. 13B shows the approximate error of the ice transport as a function of grid  
 964 refinement for the second-order P2-P1 and P2-E1 grids in transformed Stokes Test B  
 965 calculations, together with similar results for the first-order P1-E0 grid from Fig. 3, for  
 966 comparison. We note that both second order models show approximately the same error  
 967 at resolution  $r = 16$  as the first order P1-E0 model at resolution  $r = 40$ , and similarly for  
 968 coarser resolutions such as  $r = 8$  and  $r = 20$ , respectively. However, it is safe to say that  
 969 these second-order calculations are considerably more expensive than the first-order  
 970 calculations at comparable resolution or accuracy.



971  
 972 **Figure 13.** Comparing second-order discretizations based on the P2-P1 and P2-E1  
 973 elements from panel A to first-order discretizations using the P1-E0 element running Test  
 974 B with  $L=10$  km. Only transformed Stokes calculations are compared; standard Stokes  
 975 results behave similarly. Panel B compares the convergence and accuracy of the various  
 976 schemes with increasing resolution, while panels C, D compare the horizontal velocities  
 977 at medium and maximum resolutions.

978

979 Panels C, D in Fig. 13 compare the  $u$ -velocities from several Test B calculations  
 980 using the two second-order models in comparison with first-order P1-E0 model results  
 981 from Fig. 3. Each panel shows results from the upper surface ( $\sigma = 100\%$ ) in solid lines  
 982 and results from a surface a quarter of the way up from the bottom ( $\sigma = 25\%$ ) in dashed  
 983 lines. Panel C shows results from medium resolution calculations ( $r = 8, 20$  in the  
 984 second-order and first-order calculations, respectively) and panel D shows the  
 985 corresponding results from the higher resolution calculations ( $r = 16, 40$ ). At these  
 986 resolutions the accuracy of the first- and second-order calculations is very similar so for  
 987 clarity the second-order results are displaced horizontally from the first-order results by  
 988 0.05 nondimensional units. The P2-E1 results in magenta are displaced to the left and the  
 989 P2-P1 results in blue are displaced to the right. In general, models satisfying the  
 990 solvability condition, namely the P1-E0 and P2-E1 models, are better behaved than the  
 991 P2-P1 model. This is possibly related to the well-known “weak” mass conservation of  
 992 the Taylor-Hood element. This problem is greatly improved by “enriching” the pressure

993 space with constant pressures in each triangular element (Boffi et al., 2012). In the 2D  
 994 Test B problem this increases the number of pressure variables from  $n_p = n(m+1)$  in the  
 995 basic Taylor-Hood element to  $n(3m+1)$ , much closer to the  $4nm$  needed to satisfy the  
 996 solvability condition. On the other hand, the pressure in the P2-E1 case is highly  
 997 oscillatory but well behaved in the P2-P1 case. However, this is not at all concerning  
 998 since the transformed pressure, a Lagrange multiplier, has no physical significance.  
 999

## 1000 **8. A Summary and Discussion**

1001

1002 **In summary, this paper presents two innovations in ice sheet modeling. The first involves**  
 1003 **a transformation of the ice sheet Stokes equations into a form that differs from the**  
 1004 **approximate Blatter-Pattyn system by a small number of terms. In particular, the**  
 1005 **variational formulations differ only by the absence of terms involving the vertical**  
 1006 **velocity  $w$  in the second invariant of the strain rate tensor in the Blatter-Pattyn system.**

1007

1008 **We focus on two applications of the new transformation. The first is that these**  
 1009 **extra terms in the transformed Stokes equations may be “switched” on or off to convert**  
 1010 **the code from a full-Stokes model to a Blatter-Pattyn model, if desired. Ice sheet flow is**  
 1011 **generally shallow but often contains limited areas where Stokes equations must be**  
 1012 **solved. Thus, the switch from Blatter-Pattyn to Stokes may be done locally and**  
 1013 **adaptively only where the extra accuracy is required.**

1014

1015 **The fact that neglecting the vertical velocity in only one localized place creates**  
 1016 **the Blatter-Pattyn approximation suggests that approximating the vertical velocity instead**  
 1017 **will create improved approximations. We present two such approximations. The first**  
 1018 **approximation, called the BP+ approximation, solves the pressure-free horizontal**  
 1019 **momentum equation with the vertical velocity obtained from the continuity equation.**  
 1020 **Remarkably, this approximation turns out to be the same as a model originally proposed**  
 1021 **by Herterich (1987). An intriguing idea would be to replace the BP with the BP+**  
 1022 **approximation in the adaptive switching method. The second approximation simply**  
 1023 **approximates the vertical velocity by discretizing the continuity equation on a coarser**  
 1024 **grid than the rest of the model.**

1025

1026 **The second innovation involves the introduction and use of finite element**  
 1027 **discretizations that feature a decoupled invertible continuity equation permitting the**



1028 numerical solution for the vertical velocity in terms of the horizontal velocity  
1029 components, i.e.,  $w = w(u, v)$ . Some examples of such grids for use in 2D and 3D are  
1030 given in Appendix B. An important example is the P1-E0 grid that is used in most of the  
1031 test problems in this paper. However, one can alternatively obtain  $w = w(u, v)$  by other  
1032 means, as for example by discretizing (43). For example, this is done in MALI (Hoffman  
1033 et al., 2018), a code based on the Blatter-Pattyn approximation, to obtain the vertical  
1034 velocity  $w$  for the advection of ice temperature (Mauro Perego, private communication).  
1035

1036 Finally, no cost comparisons have been presented because the present calculations  
1037 are only proof of concept, made on a personal computer using the program Mathematica.  
1038 This is not at all representative of the computer hardware or the methods used in practical  
1039 ice sheet modeling. Furthermore, no effort was made to optimize the calculations or to  
1040 take advantage of parallelization. As a result, cost comparisons would be inaccurate and  
1041 possibly misleading.

1042

#### 1043 **Code Availability**

1044

1045 All calculations were made using the Wolfram Research, Inc. program Mathematica in a  
1046 development environment. No production code is available.

1047

#### 1048 **Competing Interests**

1049

1050 The author has acknowledged that there are no competing interests.

1051

#### 1052 **Acknowledgements**

1053

1054 I am grateful to Steve Price for support, and especially to Mauro Perego, William (Bill)  
1055 Lipscomb, and reviewers Ed Bueler and Christian Schoof for many helpful comments  
1056 and suggestions that helped to improve the paper.

1057

1058 **References**

1059

1060 Auricchio, F., da Veiga, L.B., Brezzi, F., and Lovadina, C.: Mixed Finite Element  
1061 Methods, In Encyclopedia of Computational Mechanics Second Edition (Eds E. Stein, R.  
1062 de Borst, and T.J.R. Hughes), John Wiley & Sons, Ltd., 2017.

1063

1064 Blatter, H.: Velocity and Stress Fields in Grounded Glaciers: A Simple Algorithm for  
1065 Including Deviatoric Stress Gradients, *J. Glaciol.*, 41, 333-344, 1995.

1066

1067 [Boffi, D., Brezzi, F., Fortin, M.: Finite Elements for the Stokes Problem. In: Boffi D.,  
1068 Gastaldi L. \(eds\) Mixed Finite Elements, Compatibility Conditions, and Applications.  
1069 Lecture Notes in Mathematics, vol 1939. Springer, Berlin, Heidelberg.  
1070 \[https://doi.org/10.1007/978-3-540-78319-0\\\_2\]\(https://doi.org/10.1007/978-3-540-78319-0\_2\), 2008.](#)

1071

1072 Boffi, D., Cavallini, N., Gardini, F., and Gastaldi, L.: Local Mass Conservation of Stokes  
1073 Finite Elements, *J. Sci. Comput.*, 52, 383–400, 2012.

1074

1075 [Chen, Q., Gunzburger, M., and Perego, M.: Well-Posedness Results for a Nonlinear  
1076 Stokes Problem Arising in Glaciology, \*SIAM J. Math. Anal.\*, 45\(5\), 2710-2733, 2013.](#)

1077

1078 Cheng, G., Lötstedt, P., and von Sydow, L.: A Full Stokes Subgrid Scheme in Two  
1079 Dimensions for Simulation of Grounding Line Migration in Ice Sheets Using Elmer/ICE  
1080 (v8.3), *Geosci. Model Dev.*, 13, 2245-2258, 2020.

1081

1082 Dukowicz, J.K., Price, S.F., and Lipscomb, W.H.: Consistent Approximations and  
1083 Boundary Condition for Ice Sheet Dynamics from a Principle of Least Action, *J. Glaciol.*,  
1084 56, 480-496, 2010.

1085

1086 Dukowicz, J.K., Price, S.F., and Lipscomb, W.H.: Incorporating Arbitrary Basal  
1087 Topography in the Variational Formulation of Ice Sheet Models, *J. Glaciol.*, 57, 461-467,  
1088 2011.

1089

1090 Dukowicz, J.K.: Reformulating the Full-Stokes Ice Sheet Model for a More Efficient  
1091 Computational Solution, *The Cryosphere*, 6, 21-34, 2012.

1092

- 1093 Elman, H.C., D.J. Silvester, and A.J. Wathen, 2014: *Finite Elements and Fast Iterative*  
1094 *Solvers: With Applications in Incompressible Fluid Dynamics*, 2nd Ed., Oxford  
1095 University Press, 494 pp.  
1096
- 1097 Gagliardini, O., and Zwinger, T.: The ISMIP-HOM Benchmark Experiments Performed  
1098 Using the Finite-Element Code Elmer, *The Cryosphere*, 2, 67–76, 2008.  
1099
- 1100 Gagliardini, O., Zwinger, T., Gillet-Chaulet, F., Durand, G., Favier, L., de Fleurian, B.,  
1101 Greve, R., Malinen, M., Martín, C., Råback, P., Ruokolainen, J., Sacchetti, M., Schäfer,  
1102 M., Seddik, H., and Thies, J.: Capabilities and Performance of Elmer/Ice, a New-  
1103 Generation Ice Sheet Model, *Geosci. Model Dev.*, 6, 1299–1318, doi:10.5194/gmd-6-  
1104 1299-2013, 2013.  
1105
- 1106 Greve, R. and Blatter, H.: *Dynamics of Ice Sheets and Glaciers*, Springer-Verlag, Berlin  
1107 Heidelberg, 2009.  
1108
- 1109 Heinlein, A., Perego, M., and Rajamanickam, S.: FROSch Preconditioners for Land Ice  
1110 Simulations of Greenland and Antarctica, *SIAM J. Sci. Comput.*, 44, V339-B367, doi:  
1111 10.1137/21M1395260, 2022.  
1112
- 1113 [Herterich, K.: On the Flow Within the Transition Zone Between Ice Sheet and Ice Shelf,](#)  
1114 [in \*Dynamics of the West Antarctic Ice Sheet, Proceedings of a workshop held in Utrecht,\*](#)  
1115 [May 6-8, 1985, \(Eds. C. J. Van Der Veen and J. Oerlemans\), D. Reidel, Dordrecht, 185-](#)  
1116 [202, 1987.](#)  
1117
- 1118 Hoffman, M. J., Perego, M., Price, S. F., Lipscomb, W. H., Zhang, T., Jacobsen, D.,  
1119 Tezaur, I., Salinger, A. G., Tuminaro, R., and Bertagna, L.: MPAS-Albany Land Ice  
1120 (MALI): A Variable-Resolution Ice Sheet Model for Earth System Modeling Using  
1121 Voronoi Grids, *Geosci. Model Dev.*, 11, 3747–3780, doi:10.5194/gmd-11-3747-2018,  
1122 2018.  
1123
- 1124 Hood, P. and Taylor, C.: Numerical Solution of the Navier-Stokes Equations Using the  
1125 Finite Element Technique, *Comput. Fluids*, 1, 1-28, 1973.  
1126

- 1127 Larour, E., Seroussi, H., Morlighem, M., and Rignot, E.: Continental scale, high order,  
1128 high spatial resolution, ice sheet modeling using the Ice Sheet System Model (ISSM), *J.*  
1129 *Geophys. Res.*, 117, 1–20, doi:10.1029/2011JF002140, 2012.
- 1130
- 1131 Leng, W., Ju, L., Gunzburger, M., Price, S., and Ringler, T.: A Parallel High-Order  
1132 Accurate Finite Element Nonlinear Stokes Ice Sheet Model and Benchmark Experiments,  
1133 *J. Geophys. Res.*, 117, 2156–2202, doi:10.1029/2011JF001962, 2012.
- 1134
- 1135 Lipscomb, W.H., Price, S.F., Hoffman, M.J., Leguy, G.R., Bennett, A.R., Bradley, S.L.,  
1136 Evans, K.J., Fyke, J.G., Kennedy, J.H., Perego, M., Ranken, D.M., Sacks, W.J., Salinger,  
1137 A.G., Vargo, L.J., and Worley, P.H.: Description and Evaluation of the Community Ice  
1138 Sheet Model (CISM) v. 2.1, *Geosci. Model Dev.*, 12, 387-424, 2019.
- 1139
- 1140 Nowicki, S.M.J. and Wingham, D.J.: Conditions for a Steady Ice Sheet-Ice Shelf  
1141 Junction, *Earth Planet. Sci. Lett.*, **265**(1-2), 246-255, 2008.
- 1142
- 1143 Pattyn, F.: A New Three-Dimensional Higher-Order Thermomechanical Ice Sheet  
1144 Model: Basic Sensitivity, Ice Stream Development, and Ice Flow across Subglacial  
1145 Lakes, *J. Geophys. Res.*, 108(B8), 2382, 2003.
- 1146
- 1147 Pattyn, F., Perichon, L., Aschwanden, A., Breuer, B., de Smedt, B., Gagliardini, O.,  
1148 Gudmundsson, G.H., Hindmarsh, R.C.A., Hubbard, A., Johnson, J.V., Kleiner, T.,  
1149 Konovalov, Y., Martin, C., Payne, A.J., Pollard, D., Price, S., Ruckamp, M., Saito, F.,  
1150 Soucek, O., Sugiyama, S., and Zwinger, T.: Benchmark Experiments for Higher-Order  
1151 and Full-Stokes Ice Sheet Models (ISMIP–HOM), *The Cryosphere*, 2, 95-108, 2008.
- 1152
- 1153 Perego, M., Gunzburger, M., and Burkardt, J.: Parallel Finite-Element Implementation  
1154 for Higher-Order Ice-Sheet Models, *J. Glaciol.*, 58, 76-88, 2012.
- 1155
- 1156 Rückamp, M., Kleiner, T., and Humbert, A.: Comparison of ice dynamics using full-  
1157 Stokes and Blatter-Pattyn approximation: application to the Northeast Greenland Ice  
1158 Stream, *The Cryosphere*, 16, 1675-1696, 2022.

- 1159
- 1160 Schoof, C.: Coulomb friction and other sliding laws in a higher order glacier flow model,  
 1161 Math. Models. Meth. Appl. Sci., 20(1), 157–189, 2010.
- 1162
- 1163 Schoof, C. and Hewitt, I.: Ice-Sheet Dynamics, Annu. Rev. Fluid Mech., 45, 217–239,  
 1164 2013.
- 1165
- 1166 Schoof, C. and Hindmarsh, R.C.A.: Thin-Film Flows with Wall Slip: An Asymptotic  
 1167 Analysis of Higher Order Glacier Flow Models, Quart. J. Mech. Appl. Math, 63, 73–114,  
 1168 2010.
- 1169
- 1170 Seroussi, H., Ben Dhia, H., Morlighem, M., Latour, E., Rignot, E., and Aubry, D.:  
 1171 Coupling Ice Flow Models of Varying Orders of Complexity with the Tiling Method, J.  
 1172 Glaciol., 58, 776–786, 2012.
- 1173
- 1174 Tezaur, I. K, Perego, M., Salinger, A. G., Tuminaro, R. S., and Price, S. F.:  
 1175 Albany/FELIZ: A Parallel, Scalable and Robust, Finite Element, First-Order Stokes  
 1176 Approximation Ice Sheet Solver Built for Advanced Analysis, Geosci. Model Dev., 8,  
 1177 1197–1220, 2015.

1178

## 1179 **Appendix A: Test Problems**

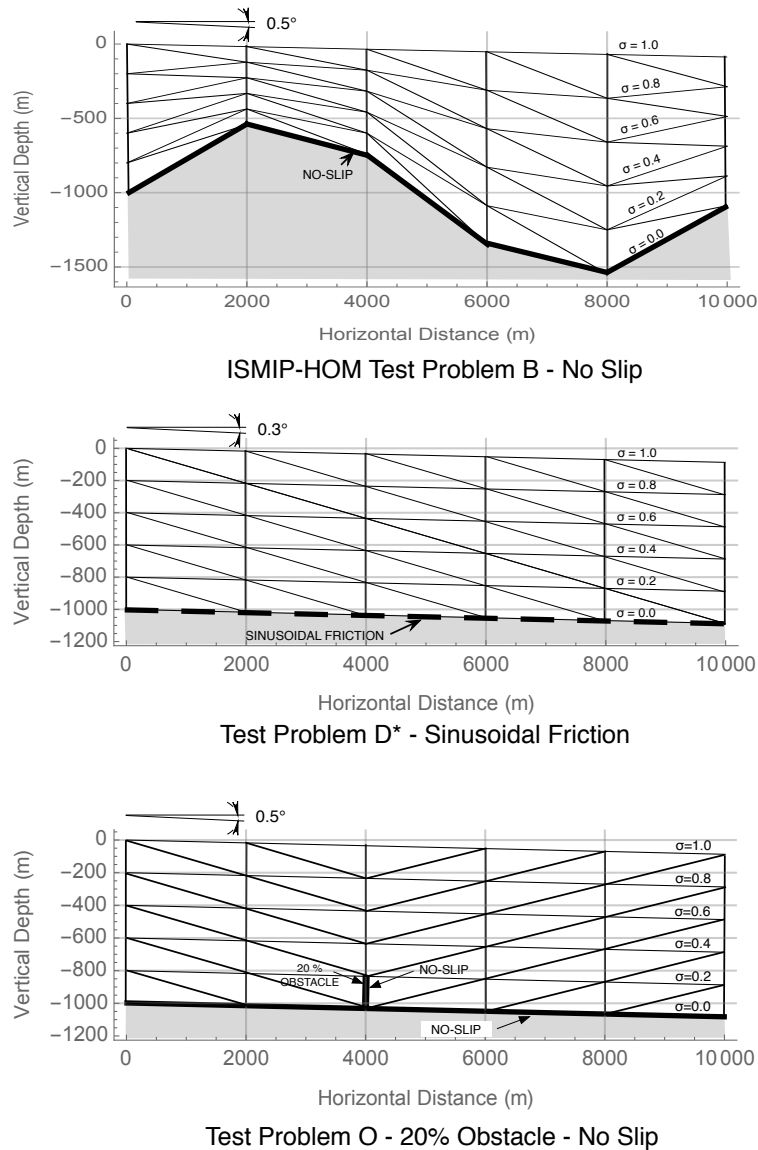
1180

1181 We will use three 2D test problems to demonstrate the new methods. The geometrical  
 1182 configuration of the three problem grids is illustrated in Fig. A1. The first problem, Test  
 1183 B, is actually Exp. B from the ISMIP-HOM benchmark suite (Pattyn et al., 2008); it  
 1184 features a no-slip condition (infinite friction) on a sinusoidal basal surface. The second  
 1185 problem, Test D\*, incorporating sinusoidal friction along a uniformly sloped plane basal  
 1186 surface, is a replacement with modified parameters for Exp. D from the benchmark suite  
 1187 since ice flow in Exp. D is nearly vertically uniform (see Fig. 4), more characteristic of a  
 1188 shallow-shelf approximation, and this is rectified by increased basal friction.

1189

1190 A third problem, Test O (for “Obstacle”) is introduced to the illustrate adaptive  
 1191 switching discussed in §6.1. Test O has a unique feature, namely, a thin no-slip obstacle,  
 1192 located at  $x = 4 \text{ km}$  and extending vertically  $200 \text{ m}$  from the bed (20 % of the ice sheet  
 1193 thickness), as illustrated in Fig. A1, which forces the ice flow near the obstacle to adjust

1194 abruptly. Because of the no-slip boundary conditions along the obstacle surface, a  
 1195 triangular element in the lee of the obstacle, with one vertical edge and one edge along  
 1196 the bed, would have all zero vertex velocities. This implies zero stress and therefore a  
 1197 local singularity in ice viscosity. To avoid this, all elements at the back of the obstacle  
 1198 are “reversed” as compared to the ones at the front of the obstacle, as shown in Fig. A1.  
 1199



1200  
 1201 **Figure A1.** Test problem grids. For clarity, a coarse 5x5 configuration is shown.  
 1202

1203 All tests feature a sloping flat upper surface, given by  $z_s(x) = -x \tan(\theta)$ , where  
 1204  $\theta = 0.5^\circ$  for Tests B and O, and  $\theta = 0.3^\circ$  for Test D\* (this differs from the  $0.1^\circ$  slope in  
 1205 Test D), with a free-stress upper boundary condition in all cases. The sinusoidal bottom

1206 surface elevation for Test B is specified by  $z_b(x) = z_s(x) - H_0 + H_1 \sin(\omega x)$ , where the  
 1207 depth  $H_0 = 1000 \text{ m}$ ,  $H_1 = 500 \text{ m}$ ,  $\omega = 2\pi/L$ , and  $L$  is the perturbation wavelength,  
 1208 which is also the domain length. The bottom surface elevation in Tests D\* and O is  
 1209  $z_b(x) = z_s(x) - H_0$ , parallel to the upper surface. The length  $L$  in the ISMIP-HOM suite  
 1210 ranges from  $5 \text{ km}$  to  $160 \text{ km}$ , but here we consider only the two cases at the high end of  
 1211 the aspect ratio  $H_0/L$  range, namely,  $L = 5 \text{ km}$  and  $L = 10 \text{ km}$ , where the inaccuracy of  
 1212 the Blatter-Pattyn approximation becomes noticeable. In all cases the lateral boundary  
 1213 conditions are periodic. The spatially varying friction coefficient for Test D\* is given by  
 1214  $\beta(x) = \beta_0 + \beta_1 \sin(\omega x)$ , where  $\beta_0 = \beta_1 = 10^4 \text{ Pa a m}^{-1}$  (these are an order of magnitude  
 1215 higher than in Test D). The physical parameters are the same as in ISMIP-HOM,  
 1216 namely, ice-flow parameter  $A = 10^{-16} \text{ Pa}^{-3} \text{ a}^{-1}$ , ice density  $\rho = 910 \text{ kg m}^{-3}$ , and  
 1217 gravitational constant  $g = 9.81 \text{ ms}^{-2}$ . In general, units are MKS, except where time is  
 1218 given per annum, convertible to per second by the factor  $3.1557 \times 10^7 \text{ s a}^{-1}$ .

1219

## 1220 **Appendix B: Grids Satisfying the Solvability Condition**

### 1221 **B1 An Invertible Continuity Equation**

1222

1223 As discussed in §4, the invertibility of the discrete continuity equation requires special  
 1224 grids that satisfy the solvability condition. Here we discuss several such grids and their  
 1225 properties. Fig. B1 shows three 2D elements on triangles or quadrilaterals that satisfy the  
 1226 solvability condition (57) in certain circumstances. The P1-E0 element is quite general,  
 1227 as demonstrated in §B2. It has velocities located at triangle vertices, resulting in a linear  
 1228 velocity distribution within each triangle (P1), and pressure located on the vertical edge  
 1229 of each triangle, providing a constant pressure over the two triangles that share that edge  
 1230 (E0). A second order version of this element, the P2-E1 element, is shown in Fig. 13A.  
 1231 The other two elements, the P1-Q0 and Q1-Q0 elements, satisfy the solvability condition  
 1232 when used in Tests B and D\* but may not do so in other problems. The P1-Q0 element  
 1233 also has velocities on triangle vertices for a linear velocity distribution within each  
 1234 triangle (P1) but the pressure is constant within the quadrilateral (Q0) formed by the two  
 1235 adjoining triangles. The Q1-Q0 element has velocities located at quadrilateral vertices  
 1236 and pressure centered in the quadrilateral, resulting in a bi-quadratic velocity distribution  
 1237 (Q1) and a constant pressure within the quadrilateral (Q0).

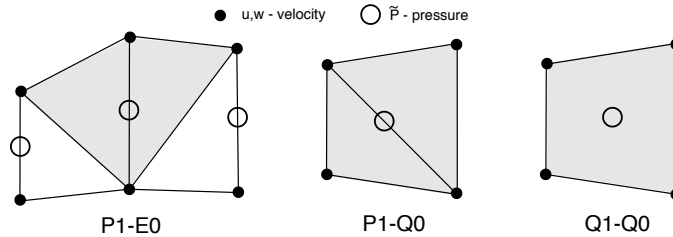


**Figure B1.** Three first-order 2D elements that may be used to satisfy the solvability condition, (57), in Tests B and D\*.

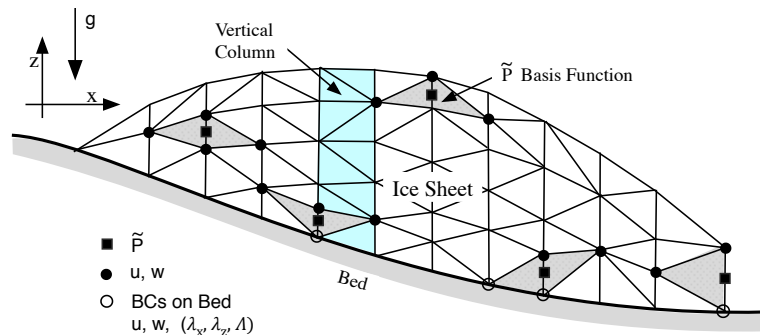
The solutions are stable, as expected, and they all converge with the same value for ice transport. The pressure distribution is smooth in the P1-E0 case, but contains small fluctuations near the upper surface in the P1-Q0 and Q1-Q0 cases that tend to disappear as resolution is increased. The Q1-Q0 element is unstable in conventional applications because it contains a checkerboard pressure null space and is only used in a stabilized form (see Elman et al., 2014, where the element is called Q1-P0). Here, however, the Q1-Q0 grid does behave well, presumably because it satisfies the solvability condition. Overall, this confirms our expectation of stability when the solvability condition is satisfied. As we discuss next, the P1-E0 element is special because the solvability condition is satisfied along each vertical edge, as opposed to being satisfied over the entire grid as in the other two elements.

## B2 The Solvability Condition in the P1-E0 Element

Fig. B2 illustrates the P1-E0 element used in a representative grid. We assume that the grid is composed of vertical columns subdivided into triangular elements. Consider a single vertical edge from bottom to the top. Assuming there are  $m$  edge segments in the vertical direction, there will be  $m+1$  discrete  $w$  variables and  $m$  discrete  $\tilde{P}$  variables since each  $\tilde{P}$  variable is located between a pair of  $w$  variables. However, since the  $w$  variable at the bed is specified as a boundary condition, either directly as a no-slip condition or as part of a no-penetration condition, there will be only  $m$  unknown  $w$  variables. As a result we have  $n_w = n_p$  along each vertical grid edge, and therefore over the entire grid, satisfying the solvability condition. In case Lagrange multipliers are used, there will be  $m+1$  unknown discrete  $w$  variables (since now the basal vertical velocity  $w$  is also an unknown). However, this is matched by  $m$  unknown  $\tilde{P}$  variables, supplemented by one  $\lambda_z$  or one  $\Lambda$  unknown Lagrange multiplier variable, depending on the type of boundary condition. Thus, again the number of unknown variables equals the



1268 number of equations along every vertical edge, thereby satisfying the solvability  
 1269 condition whether Lagrange multipliers are used or not. This means that the P1-E0  
 1270 element can be used to satisfy the solvability condition irrespective of the boundary  
 1271 conditions on quite arbitrary grids, as illustrated in Fig. B2. These arguments apply for  
 1272 other versions of the P1-E0 element as well, such as the second order version P2-E1 in  
 1273 Fig. 13A or the 3D version in Fig. B3.



1274  
 1275

1276 **Figure B2.** An illustration of a 2D edge-based P1-E0 grid, composed of vertical columns  
 1277 randomly subdivided into triangles. Pressures are located on the vertical edges.  
 1278 The triangulation and the configuration of the associated pressure basis functions  
 1279 (shown in gray) is quite general, allowing for a flexible triangulation of the domain.

1280

### 1281 **B3 Two- and Three-Dimensional Meshes Based on the P1-E0 Element**

1282 The P1-E0 element has been used on the test problem grids in Fig. A1 and  
 1283 performs well. Moreover, the element has great geometric generality, as in Fig. B2, so it  
 1284 may be used for quite complicated grids. Generally, there are two triangles associated  
 1285 with a pressure variable, one on each side of a vertical edge, except in situations where  
 1286 the ice sheet ends at a vertical face, as in Fig. B2. However, there is no problem since the  
 1287 pressure is simply associated with the single triangle on one side of the vertical face.

1288

1289 Meshes composed of P1-E0 elements have another useful property. Since  
 1290 pressure and vertical velocity variables alternate along vertical grid lines, the matrix-  
 1291 vector products  $M_{wp}p$ ,  $M_{wp}^T w$  in (47), corresponding to  $\partial \tilde{P}/\partial z$  and  $\partial w/\partial z$  in the  
 1292 vertical momentum and continuity equations, respectively, consist of simple decoupled  
 1293 bi-diagonal one-dimensional difference equations along each vertical grid line for  
 1294 determining pressure and vertical velocity. This should be particularly advantageous for  
 1295 parallelization.

1296

1297

1298

1299

1300

1301

1302

1303

1304

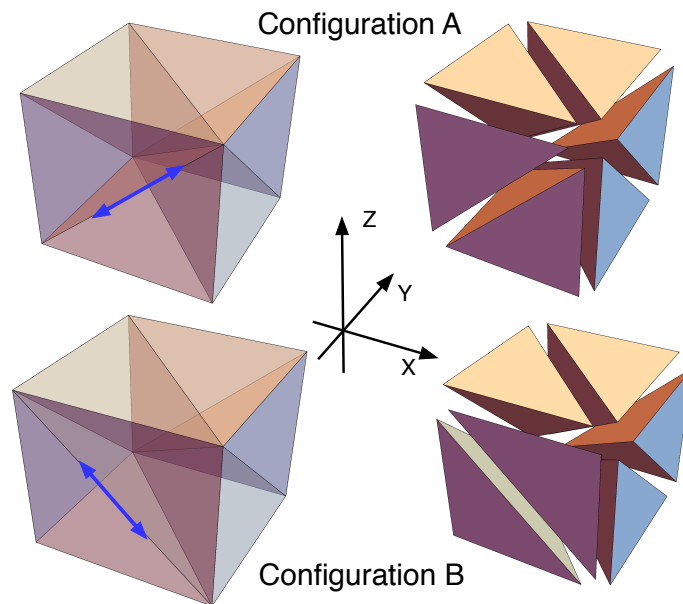
1305

1306

1307

1308

The two-dimensional P1-E0 element has a relatively simple three-dimensional counterpart, shown in Fig. B3. The mesh again consists of vertical columns, this time composed of hexahedra. Each hexahedron is subdivided into six tetrahedra such that each vertical edge is surrounded by as few as four to as many as eight tetrahedra. As in the 2D case, velocity components are collocated at vertices, yielding a piecewise-linear velocity distribution in each tetrahedral element, and pressures are located in the middle of each vertical edge so that pressure is constant in the tetrahedra that surround that edge. Lagrange multipliers, if used, are located at the vertices on the basal surface, yielding a piecewise linear distribution on the basal triangular facet. Since pressures and vertical velocities are again intermingled along a single line of vertical edges from top to bottom, we see that this satisfies the solvability condition (57) since the argument used in the 2D case applies here also.



1309

1310

1311

1312

1313

1314

**Figure B3.** Three-dimensional P1-E0 tetrahedral elements that generalize the 2D P1-E0 element of Fig. C1. Configurations A and B differ by having an internal triangular face rotated, as indicated by the blue arrows. Both configurations satisfy the solvability condition.

1315

1316

1317

1318

Fig. B3 shows two of the several possible configurations of a typical hexahedron, including an exploded view of each configuration for clarity. The two configurations differ in having the internal face of the two forward-facing tetrahedra rotated, creating two different forward facing tetrahedra. The remaining six tetrahedra are undisturbed.

1319 Since edges must align when hexahedra (or tetrahedra) are connected, this shows that the  
1320 3D mesh can be flexibly reconnected and rearranged, just as in the 2D case of Fig. B2.

1321

1322 **Remark #2:** A closely related but perhaps even simpler three-dimensional P1-E0  
1323 element is one based on the P2-P1 prismatic tetrahedral element that is used in Leng et al.  
1324 (2012). A grid of these elements is composed of vertical columns of triangular prisms,  
1325 with triangular faces at the top and bottom, which are then each subdivided into three  
1326 tetrahedra. As in Fig. B3, pressures are located on the vertical prism edges so this again  
1327 satisfies the solvability condition.

1328

1329 Just as the 2D second-order P2-E1 element in Fig. 13A is a generalization of the  
1330 P1-E0 element, a 3D second-order P2-E1 element may be constructed as a generalization  
1331 of the P1-E0 element illustrated in Fig. B3. Velocities would be located at the vertices  
1332 and at midpoints of the tetrahedral edges, and pressures halfway between the velocities  
1333 on vertical edges, including the imaginary vertical edges through the midpoints of the  
1334 tetrahedral edges, in the same way as in the 2D case in Fig. 13A. The P2-E1 element in  
1335 both 2D and 3D would also satisfy the solvability condition since the arguments in §B2  
1336 apply here as well because pressures are again located midway between vertical  
1337 velocities along all vertical edges.